CHARACTERISATION AND APPLICATION OF CARBON DOPED ALUMINIUM OXIDE OPTICALLY STIMULATED LUMINESCENCE DOSIMETER IN MEGAVOLTAGE PHOTON BEAMS FOR RADIOTHERAPY

FASIHAH HANUM BINTI MD YUSOF

FACULTY OF MEDICINE
UNIVERSITY OF MALAYA
KUALA LUMPUR

2016

CHARACTERISATION AND APPLICATION OF CARBON DOPED ALUMINIUM OXIDE OPTICALLY STIMULATED LUMINESCENCE DOSIMETER IN MEGAVOLTAGE PHOTON BEAMS FOR RADIOTHERAPY

FASIHAH HANUM BINTI MD YUSOF

DISSERTATION SUBMITTED IN FULFILMENT OF THE REQUIREMENTS FOR THE DEGREE OF MASTER OF MEDICAL PHYSICS

FACULTY OF MEDICINE
UNIVERSITY OF MALAYA
KUALA LUMPUR

2016

UNIVERSITI MALAYA

ORIGINAL LITERARY WORK DECLARATION

Name of Candidate: Fasihah Hanum binti Md Yusof (I.C/Passport No:)

Registration/Matric No: MGQ130010

Name of Degree: Master of Medical Physics

Title of Project Paper/Research Report/Dissertation/Thesis ("this Work"): Characterisation and Application of Carbon Doped Aluminium Oxide Optically Stimulated Luminescence Dosimeter in Megavoltage Photon Beams for Radiotherapy

Field of Study: Medical Physics

I do solemnly and sincerely declare that:

(1) I am the sole author/writer of this Work;
(2) This Work is original;
(3) Any use of any work in which copyright exists was done by way of fair dealing and for permitted purposes and any excerpt or extract from, or reference to or reproduction of any copyright work has been disclosed expressly and sufficiently and the title of the Work and its authorship have been acknowledged in this Work;
(4) I do not have any actual knowledge nor do I ought reasonably to know that the making of this work constitutes an infringement of any copyright work;
(5) I hereby assign all and every rights in the copyright to this Work to the University of Malaya ("UM"), who henceforth shall be owner of the copyright in this Work and that any reproduction or use in any form or by any means whatsoever is prohibited without the written consent of UM having been first had and obtained;
(6) I am fully aware that if in the course of making this Work I have infringed any copyright whether intentionally or otherwise, I may be subject to legal action or any other action as may be determined by UM.

Candidate's Signature Date 9 March 2016

Subscribed and solemnly declared before,

Witness's Signature Date 9 March 2016

Name:
Designation:

ABSTRACT

Radiotherapy is long recognised as a method to treat cancer. In recent years, advanced radiotherapy techniques such as intensity modulated radiation therapy (IMRT) and volumetric modulated arc therapy (VMAT) has been introduced. These techniques allows the delivery of escalated radiation dose with better target conformity, which leads to the needs of precise and accurate treatment verification to ensure the correct dose is being delivered to the target during radiotherapy. Besides the pre-treatment quality assurance, *in-vivo* dose verification may be needed. Optically stimulated luminescence dosimeter (OSLD) is a relatively new dosimeter which uses light photons to stimulate the release of dosimetric traps.

This study covers the characterisation and application of the OSLD in selected radiotherapy techniques. The first part of this study investigated the physical characteristics of the OSLD for dosimetry under megavoltage photon beams. The OSLD were tested for different energies, repetition rates, field sizes, source to surface distances (SSD), and beam incident angles. The linearity, reproducibility, fading effect, signal depletion per readout and the effect of cumulative dose of the OSLD were also investigated. The OSLD demonstrated good linearity and reproducibility, stable after nine minutes post-irradiations, small signal depletion per readout (0.03%), small dependence of energy (≤5.23%), repetition rate (≤2.60%), SSD (≤2.34%), field size (≤5.23%) and angularity (≤3.50%).

For practicality, detectors are often placed on the skin of patient for *in-vivo* dose measurement. In the second part of this study, the suitability of using the OSLD in measuring surface dose during radiotherapy was investigated. The water equivalent depth (WED) of the OSLD was first determined followed by comparisons of surface dose measured on a solid water phantom using the OSLD, which was benchmarked

against measurements using the Markus ionization chamber and Gafchromic EBT3 film. The OSLD was also used to measure surface of a cohort of 10 patients undergoing conventional 3D conformal breast radiotherapy to evaluate its feasibility and accuracy in real clinical setup. The OSLD has a WED of 0.4 mm depth which consequently overestimated the surface dose by a factor of 2.37 for 6 MV and 2.01 for 10 MV photon beams, respectively.

In the third part of the study, the OSLD was used for dosimetric verification of treatment plans namely 3D-CRT, IMRT and VMAT. Three plans were generate in 3D-CRT treatment planning which are single field, opposed fields and 4-fields. In IMRT and VMAT, two plans were generated simulating head and neck and prostate cases. The OSLD measurements were compared to TPS predicted dose. The uncertainty of the measurement was found to be within 3.16 ± 2.20% at the region where the dose is homogeneous. At the slight dose gradient region, the uncertainty was expected to be within 6.4 ± 4.2% and at regions where large dose gradients exist, the uncertainty was expected to increase to 9.0 ± 6%.

In conclusion, the OSLD was found to be suitable to be used as a dosimeter for megavoltage photon beams. However, due to the finite size of the detector, the measurement uncertainties increase with the complexity of the treatment techniques.

ABSTRAK

Radioterapi telah terkenal sebagai satu kaedah untuk merawat barah. Kontemporari kini, kaedah radioterapi moden seperti intensiti modulasi radioterapi (IMRT) dan volumetrik modulasi radioterapi (VMAT) telah diperkenalkan. Kaedah baru ini membolehkan penyampaian dos radiasi yang tinggi dengan mengikut kawasan sasaran yang lebih tepat. Jadi, pengesahan dos perubatan yang tepat diperlukan bagi memastikan dos yang betul diberikan kepada kawasan sasaran semasa radioterapi. Selain daripada jaminan kualiti pra-rawatan yang biasa, pengesahan dos secara *in-vivo* juga diperlukan. 'Optically stimulated luminescence dosimeter' (OSLD) ialah dosimeter baharu yang menggunakan cahaya foton untuk merangsang pembebasan elektron daripada perangkap dosimetri.

Kajian ini merangkumi pencirian dan penggunaan OSLD dalam kaedah radioterapi yang terpilih. Dalam bahagian pertama kajian ini, pencirian fizikal bagi kegunaan alur foton megavoltan OSLD telah dilaksanakan. Pergantungan dosimeter tersebut terhadap tenaga, kadar pengulangan, saiz bidang, jarak punca ke permukaan dan sudut pancaran alur, telah dikaji. Selain itu, kelinearan, kebolehulangan, kesan pengurangan selepas diradiasi, tindakbalas terhadap bacaan berulang dan kesensitifan terhadap dos terkumpul OSLD telah dikaji. OSLD menunjukkan tahap kelinearan dan kebolehulangan yang baik, stabil sembilan minit selepas diradiasi, mempunyai isyarat berkurangan yang sedikit selepas setiap bacaan (0.03%), mempunyai pergantungan yang kecil terhadap tenaga (≤5.23%), kadar pengulanagan (≤2.60%), jarak punca ke permukaan (≤2.34%), saiz bidang (≤5.23%) and sudut pancaran alur (≤3.50%).

Secara praktikal, dosimeter selalunya diletakkan di atas permukaan kulit pesakit dalam pengukuran dos *in-vivo*. Dalam bahagian kedua kajian ini, kesesuaian OSLD dalam mengukur dos permukaan semasa radioterapi telah dikaji. Persamaan kedalaman

air bagi OSLD telah dikaji dan dos permukaan yang diukur menggunakan OSLD di atas pemukaan fantom air pepejal telah dibandingkan dengan dos permukaan yang diukur mengunakan kebuk pengionan Markus dan filem Gafchromic EBT3. Kesan sudut pancaran alur juga telah dikaji. Selain itu, OSLD juga telah digunakan dalam mengukur dos permukaan bagi 10 pesakit yang menjalani rawatan 3D konvensional radioterapi payudara bersudut bagi menilai kebolehlaksanaan serta ketepatannya dalam kegunaan klinikal. OSLD mempunyai persamaan kedalam air sebanyak 0.4mm di mana ia mengakibatkan pengukuran dos permukaan yang berlebihan sebanyak faktor 2.37 bagi 6 MV dan 2.01 bagi 10 MV alur foton.

Penggunaan OSLD dalam kaedah IMRT dan VMAT juga telah diterokai dalam bahagian terakhir kajian ini. Tiga pelan telah dibuat bagi 3D-CRT merangkumi pelan satu bidang, dua bidang dan empat bidang. Bagi IMRT dan VMAT, dua pelan telah dibuat mensimulasi kes kepala dan leher serta prostat. Bacaan OSLD telah dibandingkan dengan jangkaan dos TPS. Ralat bacaan dijangka dalam julat 3.16 ± 2.20% bagi kawasan yang mempunyai serakan dos yang sekata.Bagi kawasan yang wujudnya kecerunan dos yang sedikit, ralat bacaan dijangkakan dalam julat 6.4 ± 4.2%. dan ralat bacaan dijangka meningkat sehingga 9.0 ± 6% bagi kawasan berkecuranan dos tinggi.

Kesimpulannya, OSLD sesuai digunakan sebagai dosimeter bagi alur foton megavoltan. Walau bagaimanapun, disebabkan saiz detektor yang terhad, ralat dalam pengukuran dos akan meningkat ekoran daripada teknik rawatan yang semakin kompleks.

ACKNOWLEDGEMENT

By His will and favor, I finally succeed in completing research and dissertation entitled 'Characterisation and application of optically stimulated luminescence dosimeter (OSLD) in megavoltage photon beams for radiotherapy'. Firstly, I would like to express my admiration and appreciation to my family who have encouraged me to further my study in master degree. I would like to express my heartfelt gratitude to my supervisors, Dr. Ung Ngie Min and Dr. Jeannie Wong Hsiu Ding, for their endless help and extending their valuable knowledge to me while completing my study. Furthermore, I would like to extend my appreciation to the staffs of Clinical Oncology Unit, University of Malaya Medical Centre, for their help and support during the collecting data process. I also would like to thank Dr. Heng Siew Ping, a senior physicist at Pantai Hospital Kuala Lumpur, Mr. Jong Wei Loong and Mr. Vannyat Ath who always helped me with my measurements. Last but not least, a special thanks to all the people involved for their unconditional and untiring help throughout the progression of this dissertation.

TABLE OF CONTENTS

LIST OF FIGURES

LIST OF TABLES

LIST OF SYMBOLS AND ABBREVIATIONS

3D-CRT	Three dimensional conformal radiation therapy
AAPM	American Association of Physicists in Medicine
CT	Computed tomography
DNA	Deoxyribonucleic acid
EBRT	External beam radiation therapy
ETAR	Equivalent tissue air ratio
ICRU	*International Commission on Radiation Units & Measurements*
ICRP	*International Commission on Radiological Protection*
IGRT	Image guided radiation therapy
IMRT	Intensity modulated radiation therapy
LED	Light emitting diode
LET	Linear energy transfer
MOSFET	Metal oxide semiconductor field effect transistor
OAR	Organ at risk
OD	Optical density
OSL	Optical stimulated luminescence
OSLD	Optical stimulated luminescence dosimeter
PBC	Pencil beam convolution
PDD	Percentage depth dose
PMT	Photomultiplier tube
PTV	Planning Target volume
ROI	Region of Interest
SD	Standard deviation
SSD	Source to surface distance

TL	Thermoluminescence
TLD	Thermoluminescence dosimeter
TPS	Treatment planning system
VMAT	Volumetric modulated arc therapy
WED	Water equivalent depth
WET	Water equivalent thickness

LIST OF APPENDICES

CHAPTER 1: INTRODUCTION

1.1 Overview

Radiotherapy is a treatment technique which uses high energy ionising radiation to control or kill cancer cells. This technique is able to damage the deoxyribonucleic acids (DNAs) of cancerous cells leading to cellular deaths. The surrounding healthy cells will also suffer from cell damage but they are usually able to repair themselves. The amount and type of radiation delivered is carefully planned, verified and calculated by treatment planning system (TPS) as to optimise the dose received by the cancerous cells while sparing surrounding healthy cells.

However, advanced radiotherapy techniques produce radiation dose maps with high dose modulation and tight gradients (Palma et al., 2010). As radiotherapy involves many complex processes in term of planning and treatment delivery, it leads to opportunities for error occurrence (Pisani et al., 2000; Van Herk, 2004). These errors may either results in the under-dose of the cancerous cells or unnecessary over-dosing of the organs at risk (Hunt et al., 1993). The International Commission on Radiation Units & Measurements (ICRU) recommended that the overall accuracy in dose to patient which includes absorbed dose calibration, beam data, TPS dose calculation and treatment delivery should be within ±5% (Jones, 1994). The American Association of Physicists in Medicine (AAPM) and International Atomic Energy Agency (IAEA) recommended that the acceptable criteria for external beam dose calculation in an inhomogeneous medium should be within ±7% and 7mm respectively (Fraass et al., 1998; IAEA, 2004).

In-vivo dosimetry is one of the method that can be used to detect errors, assess clinically relevant differences between planned and delivered dose, record the dose

received by individual patients as well as fulfill legal requirements of a radiotherapy treatment (Mijnheer et al., 2013). However, difficulties in the dosimetric verification of these new complex treatment methods using existing dosimeters has led to the need for a new generation dosimeters suitable for *in-vivo* dosimetry (Kutcher et al., 1994).

Recently, optical stimulated luminescence dosimeter (OSLD) which is a passive and point dosimeter has been used in clinical practice. Carbon doped aluminum oxide (Al_2O_3:C) based dosimeter has been shown to respond to the stimuli of visible light. It requires no cable, allows multiple readouts, reusable after optical bleaching, and able to simultaneously estimate accumulated and single doses with the same dosimeter, irradiated with low or high energy photons (Ismail et al., 2009; Malthez et al., 2009; Reft, 2009b).

Numerous studies have been conducted using the new commissioned OSLD (Dunn et al., 2013; Jursinic, 2007a,2010; Yukihara et al. 2008). This study characterises the Al_2O_3:C OSLD to be used under megavoltage radiotherapy and investigates the suitability of OSLD to be used in measuring surface doses as well as in dose verification using advanced radiotherapy techniques of Intensity Modulated Radiation Therapy (IMRT) and Volumetric Modulated Arc Therapy (VMAT).

1.2 Objectives of Study

This study comprises three main objectives, which are as follows:

i. To study the OSL dosimetric properties of Al_2O_3:C OSLDs subjected to megavoltage photon irradiation
ii. To verify the application of OSLD for surface dose measurement during radiotherapy

iii. To evaluate the suitability of OSLD for *in-vivo* dose verification in advanced radiotherapy techniques

1.3 Structure of The Thesis

This thesis consists of seven chapters, which are organized as follows:

Chapter 1 introduces the thesis structure, main objectives and aims of the research, along with a proper introduction of radiotherapy, focusing mainly on external beam radiation therapy (EBRT).

Chapter 2 provides a review of the literature on the basic radiation dosimetry in radiotherapy, the history of the use of OSLD, the basic principle of OSL system, some characteristics of OSLD and its Al_2O_3:C properties as well as the application of OSLD for clinical radiation dosimetry.

Chapter 3 provides an explanation on all the materials and equipments used in this study.

Chapter 4 describes the basic dosimetric characteristics of OSLD under megavoltage radiation beam. The characterisation work consists of calibration of the OSLD sensitivity, identification of the dose linearity, energy, repetition rate, SSD, angular and field size dependences, evaluation of post-irradiation fading effect, signal depletion per readout and identification of OSLD sensitivity towards cumulative dose.

Chapter 5 explores the use of OSLD in measuring surface dose during radiotherapy which includes five parts: 1) Determination of the water equivalent depth (WED) of OSLD to determine the intrinsic buildup of the dosimeter; 2) Comparison of surface dose using OSLD with other comparable detector namely Markus ionisation chamber and Gafchromic EBT3 film using the flat surface of solid water phantom; 3)

Surface dose measurement using OSLD to investigate the beam angle as a factor that may affect the surface dose; 4) Identification of the suitability of OSLD to be used in measuring dose on human curve surface specifically during breast radiotherapy using anthropomorphic phantom; and 5) Surface dose measurement on patient during breast radiotherapy.

Chapter 6 investigates the use of OSLD as a clinical *in-vivo* dosimeter to verify point dose and dose distribution for three dimensional conformal radiation therapy (3D-CRT) and advanced radiotherapy techniques such as IMRT and VMAT.

Chapter 7 presents the conclusion of this study, as well as recommendations for using OSLD under megavoltage beam dosimetry. It also discusses the limitations of the study.

CHAPTER 2: LITERATURE REVIEW

2.1 Introduction to Radiotherapy

Radiotherapy can be defined as a treatment that uses carefully calculated high energy ionising radiation (either photons such as x-rays and gamma rays or particle radiation, such as electron beams, protons and carbon ions) for cancer treatment (Mayles et al., 2010).

In Malaysia, the most common type of external radiotherapy is delivered using a machine called a 'linear accelerator'. A treatment planning process is applied before treating the patients. Dose and set up parameters are calculated and determined accurately for effective and precise treatment delivery. Nowadays, there is a dramatic increase in advanced technologies available for delivering radiotherapy. New techniques such as volumetric modulated arc therapy (VMAT), image guided radiation therapy (IGRT) and intensity modulated radiation therapy (IMRT) (Palma et al., 2010) have been introduced to improve the quality of treatment in terms of conformity of target area and minimisation of dose to the critical organ and structures (Wolff et al., 2009).

The use of radiation for treatment may cause a variety of physical skin reactions and contributes to pain, discomfort, irritation, itch and burn (McQuestion, 2006). Moreover, the skin is also at risk of skin toxicity such as erythema, necrosis, desquamation, dermal lymphatic and basal-cell carcinoma (Chang-Claude et al, 2005; Cooper et al., 2004; Vloten et al., 1987). Some acute side effects may also occur due to the irradiation from the treatment such as secondary breast cancer (Stovall et al., 2008; Yadav et al., 2008).

2.1.1 Three Dimensional Conformal Radiation Therapy (3D-CRT)

3D-CRT is a conventional technique that starts with obtaining region of interest by CT scans. The scanned images are then exported into the TPS. Using 3D visualisation of the tumours, normal adjacent structures, the radiation beam direction and intensity will be selected to construct dose distribution. 3D-CRT technique uses direct planning of TPS.

3D-CRT has several limitations as the treatment needs large numbers of beams for a complex volume of tumour and it needs a complicated plan for a concave target.

2.1.2 Intensity Modulated Radiation Therapy (IMRT)

IMRT is a type of conformal radiotherapy which was introduced in the 1990s to overcome the limitations of 3D-CRT. The IMRT functions in providing a better conformal of tumour's shape by modulating the intensity of the radiation beam in multiple small volumes. It shapes the radiation beams to be focus to the area of the target volume by using inverse planning software. IMRT divides each large radiation beam into several beam segments. The intensity of each of the beam segments will be adjusted individually which results in more conformal in dose distribution and allow for lower doses to organs at risk.

IMRT is delivered using either dynamic or step-and-shoot modes of multi-leaf collimators (Alaei et al., 2004). In dynamic mode, each leaf pairs of MLC moves continuously in unidirectional using independent speed while the beam is on (Sivakumar et al., 2008). Meanwhile, in step-and-shoot or also known as sliding window mode means that the system alternates between delivering radiation with a static MLC pattern and moving to the next pattern without irradiating (Ezzell &

Chungbin, 2001). The advantage of the IMRT over 3D-CRT is that it produces a better conformal dose distribution that maximises the dose to target volume while minimising the dose to the adjacent healthy tissues. Consequently, it leads to the more effective dose delivery as well as fewer side effects compared to the 3D-CRT technique. However, due to its complexity, IMRT needs a slightly longer treatment time as well as additional planning and safety checks before starting the treatment (van Vulpen et al., 2005).

2.1.3 Volumetric Modulated Arc Therapy (VMAT)

Basically, VMAT is an arc based therapy which is an advance technique of the IMRT technique. Unlike 3D-CRT and IMRT, VMAT allows simultaneous variation of three parameters while delivering treatment which are the gantry rotation speed, shape of the beam via movement of MLC and dose rate (Palma et al., 2010; Wolff et al., 2009). VMAT technique uses one or more arcs in treating a whole target volume depending on the complexity of the plans. The arcs require the gantry to rotate either clockwise or anti-clockwise.

The advantage of VMAT is that the treatment time is much faster compared to 3D-CRT and IMRT as well it provides a highly conformal dose distributions.

2.2 Radiation Dosimetry

Radiation dosimetry is a technique used to assess ionising radiation using a radiation dosimeter which is an instrument or device that is able to measure radiation quantity either directly or indirectly. Radiation dosimetry in radiotherapy is essential in order to measure the dose delivered to the patients accurately, and to minimize the risk

of severe side effects caused by the radiotherapy (Attix, 2008). Other than that, it is also part of the calibration, quality assurance and treatment planning to ensure accurate and precise treatment delivery (Eisenlohr & Abedin-Zadeh, 1973). It is also necessary for radiation protection of personnel.

Radiation dosimetry can be divided into two types, namely absolute dosimetry and relative dosimetry. Absolute dosimetry is a direct measure of absorbed dose of ionisation radiations under standard reference conditions and does not require dose calibration. This is different from relative dosimetry which relies on the production of a known dose exposures so that the relative opacity can be related to dose measured by a reference dosimeter. (Podgorsak, 2005).

2.3 Common Radiation Dosimeters in Radiotherapy

Radiation dosimeter is an instrument to measure radiation quantity. A combination of a dosimeter and its reader is referred to a dosimetry system. A numerous of dosimeters have been used for measuring high energy dose in radiotherapy. Every dosimeter has its own advantages and disadvantages. Thus, the requirements and conditions of the measurement must be taken into account when choosing the right dosimeter (Izewska & Rajan, 2005). Some examples of common dosimeter are gas dosimetry, thermoluminescence (TL) dosimetry, film dosimetry, semiconductor dosimetry and optically stimulated luminescence (OSL) dosimetry, which will be discussed in the following sections.

2.3.1 Ionisation chamber

An ionisation chamber is widely used as a 'gold standard' in measuring and detecting ionising radiation, as it provides a good response to radiation over a wide range of energy. The basic principle of the ionisation chamber is that, when the ionising radiation passes through the air in the chamber, it produces ion pairs. With the presence of an electric field, ion pairs are swept to the opposite charged electrodes which negative ions move to the anode and positive ions move to the cathode (Neves et al., 2012). The collection of the ion pairs at the electrodes results in an electronic current that is proportional to the number of ion pairs that have been created, hence, the radiation dose. An advantage of the ionisation chamber is that it gives a real-time response as it is an active dosimeter. However, the use of the parallel-plate ionisation chamber for *in-vivo* dosimetry is logistically impossible due to the curvature of the human body. In addition, it may require the application of many correction factors in high energy dosimetry (Gerbi & Khan, 1990; Gerbi % Khan, 1990; Rawlinson et al., 1992). An example of ionisation chamber's design is shown in Figure 2.1.

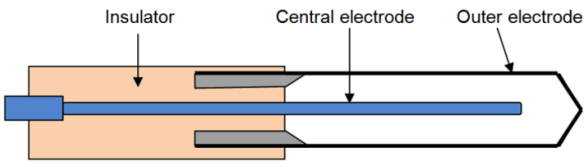

Figure 2.1: Basic design of a cylindrical type of ionisation chamber (Podgorsak Ervin, 2003)

2.3.2 Thermoluminescence Dosimeter

Basically, thermoluminescence is a temperature stimulated light emission from crystal materials after removal of electron excitation. During irradiation, free electrons are formed and the energy from ionising radiation will be absorbed which cause the electrons to excite to a higher state of conduction band. The electrons will then be dropped to trap level at the forbidden gap. The stimulation of heat will release the electrons from the meta-stable traps where the emission temperature corresponds to the energy of the defect. The electrons will then revert to their ground state and the recombination of the electrons with holes on a recombination center results in the emission of light as a thermoluminescence signal (Horowitz, 1984; McKeever et al., 1995). The illustration of stimulation and luminescence principle of TLD is shown in Figure 2.2. The amount of light emitted is proportional to the amount of radiation absorbed and it can be quantified by using a photomultiplier tube. Several materials were commonly used for a TLD such as lithium fuoride, calcium fluoride, lithium borate and calcium suplhate (J. Lee et al., 2006). Although the TLD is near tissue equivalent, the reading process is very tedious and time consuming (Chandra et al., 1982; Driscoll et al., 1986).

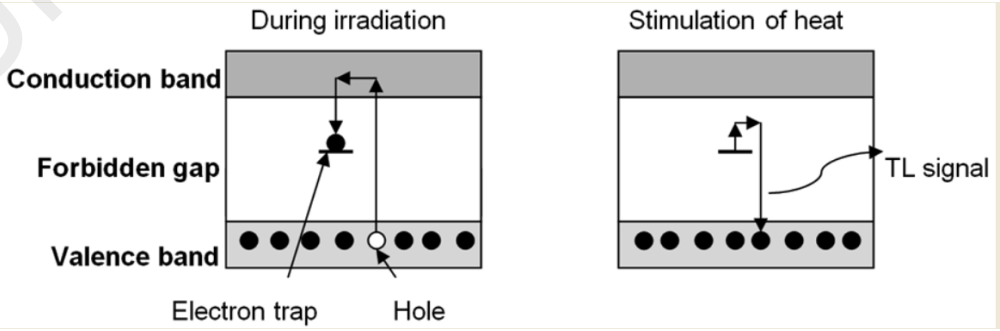

Figure 2.2: Illustration of stimulation and luminescence principle of TLD

2.3.3 Radiochromic film dosimetry

Over the years, the use of radiochromic materials in the form of films have been developed and widely used for quality assurance and radiotherapy treatment verification (Slobodan Devic, 2011). Radiochromic film has been appraised for its characteristics and uncertainties in radiotherapy using photon, electron and proton beams (Borca et al., 2013; Schembri & Heijmen, 2007). The main advantage of radiochromic film is the capability of doing two dimensional dose mapping, as opposed to the measurement of single point dose.

During irradiation, the radiochromic film which is mainly hydrophobic-substituted triphenylmethane leucocyanides polymerized by undergoing a heterolytic bond scission of the nitrile group and forms a highly coloured dye salt in the solid polymeric solution. This results in the darkening of the film. The optical density or 'blackness' of the film reflects the dose received by it (Butson et al., 2003). A radiochromic film gives a good spatial resolution (because of the molecular grains size) but is limited to the scanning resolution of the film scanner. Radiochromic film is tissue equivalent and is able to provide two-dimensional dose distribution. However, it requires a waiting period of 24 hours after irradiation before the films can be scanned to allow for post-irradiation colouration in order to achieve stability (Cheung et al. 2013; Dunn et al., 2013). The component of radiochromic film is shown in Figure 2.3.

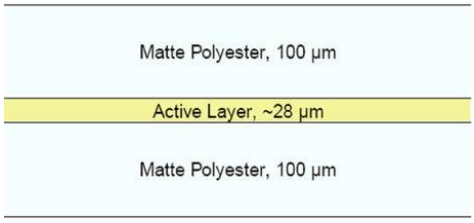

Figure 2.3: Component of radiochromic film (Maasillon et al., 2012)

2.3.4 Semiconductor dosimetry

A semiconductor diode is one of the commonly used radiation dosimeters in radiotherapy mainly due to its small size, excellent spatial resolution, and the potential for real time readout (Barbes et al. 2014; Rosenfeld, 2011). Using principle of production by taking n-type or p-type silicon and counter-doping the surface to produce the opposite type material. The p-Si type is considered more suitable for radiotherapy dosimetry because it is less affected by radiation damage and has a much smaller dark current (Podgorsak Ervin, 2003).

Physically, semiconductor diode has a depletion layer with a typical thickness in the magnitude of μm. When exposed to radiation, current will flow in the diode as a result of the production of electron-hole pairs in the depletion region (Barbés et al., 2014). Diode dosimeters can be operated with or without applying a bias voltage. Metal Oxide Semiconductor Field Effect Transistor (MOSFET) dosimeters are also another type of semiconductor dosimeter. These dosimeters are able to provide real time feedback, but usually have a water equivalent depth (WED) of 0.8 mm to 1.8 mm (Scalchi & Francescon, 1998) which exceeds the recommended dosimeter thickness of 0.07 mm, according to the International Commission on Radiological Protection (ICRP) 1991 (Fry, 1992).

2.4 Overview of Optically Stimulated Luminescence Dosimeter

2.4.1 Historical development of optically stimulated luminescence dosimetry and its application

Optically stimulated luminescence (OSL) is a response in light form emitted from an irradiated insulator or semiconductor after being exposed to light. The OSL intensity depends on the electron trapped by the radiation (Botter-Jensen et al. 2003).

OSL has been widely used in sediment or geological dating and retrospective studies. Andrew S. M. and Richard G. R (1997) used OSL in estimation of dose received during burial for individual quartz grains from an Aeolian deposit of a known age (A. S. Murray & Roberts, 1997). OSL was also used in a retrospective study by Murray A. S and Funder S. (2003) for identifying the age of coastal marine sand Eemian (A. Murray & Funder, 2003). OSLD has also been used for examining the asymmetric distribution of dose emitted by small aliquots of fluvial quartz (Olley et al., 1999). A.G. Wintle *et al.* (2006) and Madsen A.T. *et al.(*2009) investigated quartz OSL characteristics and the relevance in a single-aliquot regeneration dating protocol (Wintle et al., 2006) and young material dating using OSL respectively (Madsen & Murray, 2009).

The application of OSL in space dosimetry has also been investigated extensively. After irradiating OSL of Al_2O_3:C with selected heavy ions of ^{4}He, ^{12}C, ^{40}Ar, and ^{56}Fe, Hasuda Y. *et al.* (2001) found that OSL of Al_2O_3:C can be used as an integrating dosimetry system in future space missions as it has been proven that the angular independence and the linearity in dose response for the heavy ions were fairly good which was within ±15% (Yasuda & Kobayashi, 2001). Yukihara E. G. *et al.* (2006) reviewed recent values for relativity efficiency data for heavy charged particles as well as factors that influenced the OSL efficiencies, the linear energy transfer (LET)

dependent properties of Al_2O_3: C and the experience gained from past space experiments using Al_2O_3:C. They found that OSL of Al_2O_3:C in combination with plastic nuclear track detectors was efficient in personal dosimetry of astronauts due to its great value of LET (Yukihara et al., 2006).

Other than that, the OSL has also been used in environmental dosimetry. Jensen L. B. *et al.* (1997) proposed the use of Al_2O_3:C crystal OSL for rapid assessment of the environmental photon dose rate, and demonstrated that the Al_2O_3:C OSL with high sensitivity and energy response was ideal for measuring environmental dose rates (Botter-Jensen et al. 1997). Al_2O_3:C OSL has also been used by Kalchgrubera R. *et al.* (2002) to investigate the impact of low environmental dose rate assessment (Kalchgruber et al. 2002). Zacharias N. *et al.* (2007) carried out a study using five different types of material objectively to record environmental radiation doses by applying thermo and optically stimulated luminescence (Zacharias et al., 2007).

Furthermore, studies have also been carried out in commissioning the use of OSL as a personal dosimeter. OSL technology has proven suitable in obtaining personal dose equivalent information (S.-Y. Lee & Jai Lee, 2001). A study by Lee S. Y. *et al.* (2000) was carried out objectively to propose the uses of α-Al_2O_3:C as a new personal dosimetry system by taking advantage of its energy dependencies and optical properties (S.-Y. Lee, Kim, & Lee, 2001). The use of OSL in personal dosimetry has also been proven by Sommer M. *et al.* (2011) in their study on OSL dosimetry using beryllium oxide (Sommer et al., 2011).

The application of OSL has also spread in medical dosimetry systems (akselrod et al. 2006). The OSL system has been chosen by researchers for their studies in the radiotherapy field including external beam radiotherapy (Schembri & Hejimen, 2007; Viamonte et al., 2008; Yukihara et al., 2005) and brachytherapy (Andersen et al., 2009). It has also been characterised (Al-Senan & Hatab, 2011; Reft, 2009a) for application in

dosimetry of diagnostic radiology such as CT-scan (Funama et al., 2012; Yukihara et al., 2009) and mammography (Aznar et al., 2005).

2.4.2 Basic Principle of Optically Stimulated Luminescence Dosimeter

OSLD has shown a good response when used under high energy irradiation of radiotherapy (Dunn et al., 2013; Jursinic, 2007a; Kerns et al., 2011; Yukihara et al., 2004). Studies have demonstrated that the commercial OSL system developed by Landauer, Inc., which is also being used in this study, gave a good reproducibility that strengthens the possibility of applying the Landauer OSL commercial system in radiotherapy dosimetric procedures (Viamonte et al., 2008).

The OSL system developed by Landauer, Inc. is read out using a MicroStar reader consisting of a light source, a stimulated filter, a detection filter, and a photomultiplier tube (PMT) (Bøtter-Jensen et al., 2003). A nanoDot OSL detector containing a sensitive volume of Al_2O_3:C crystal is placed in a holder which is then inserted into the reader for the read out process. The read out process involves the stimulation of the detector by a light emitting diode (LED) array which resulted in luminescence of the crystal proportion to the amount of radiation exposed. The PMT then detects the luminescence using a high sensitivity photon counting system where a dose calculation algorithm took part in determining the exposure results using the InLight menu-driven software (McKeever et al., 2004; Viamonte et al., 2008). The number of counts, which is detected by the PMT tube, is proportional to the absorbed dose of the sensitive element of OSLDs (Perks et al., 2008).

2.4.3 Stimulation and Luminescence Theory

Stimulation and luminescence is a phenomenon of electrons being stimulated by sufficient energy and excited from the lowest energy state or ground state to a higher energy or excited state. Basically, in the principle of OSL, the electrons in the crystal material will absorb the energy from delivered irradiation which will then cause an electron-hole pair and produce the recombination center or also called F center.

The basic luminescence of OSL follows a model of two energy bands namely conduction band and valence band, separated by a forbidden band. The forbidden band localizes energy levels by defect of the crystalline structure which contains traps.

During stimulation of radiation, the charge separation of free electrons and the holes will absorb the energy and become excited. During the excitation, the electrons and holes will migrate and become trapped in an electron trap at the conduction and hole trap, and the valence bands, respectively (Jursinic, 2007b; Z. Maseeh, 2011). In addition, during the excitation, the electron that is near a defect can fall into the energy trap. Otherwise it may also cross back towards the valence band and recombine with a hole. This study uses OSLD made of Al_2O_3:C crystal and stimulation from a broad spectrum of light from 400 to 700 nm with a peak at 475 nm (Bøtter-Jensen & McKeever, 1996) which can lead the luminescence to rise from the relaxation of the excited F center with a broad emission peaking at 420 nm (J. Edmund et al., 2006; Jursinic, 2007b) and a lifetime of 35±36 ms (Akselrod et al., 2006).

The recombination of the electron and the hole will occur when the electron has enough energy to reach the conduction band. The imperfection of the lattice-impurities or defect created for the hole traps will emit light when the recombination occurs near them as the recombination energy is transferred to the luminescence center or known as

F center (J. Edmund et al., 2006). Basically, the F center for the Al_2O_3 materials that have been used in this study are mainly created by oxygen vacancies.

As the crystal is optically stimulated, the stimulation of green light leads the electrons to absorb the energy and ejected out of the trap. The electrons then will then recombine with the holes at the F^+ center. The recombination energy will transfer to a luminescence center where the light is emitted:

$F^+ + e^- \rightarrow F$ + 420 nm light

The intensity of the luminescence depends on the dose absorbed, numbers of luminescent traps that are filled, and the light intensity of the stimulation light (Jursinic, 2007a; Schembri & Heijmen, 2007).

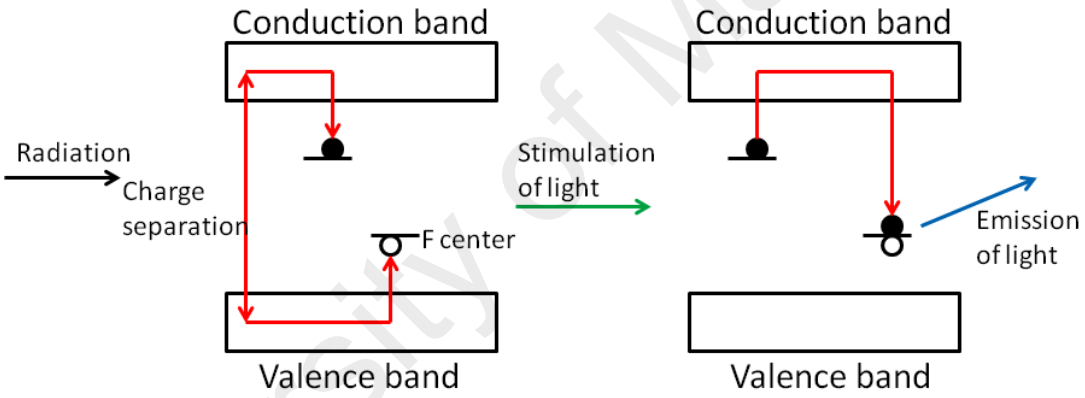

Figure 2.4: Stimulation and luminescence principle of OSLD (Jursinic, 2007b)

2.5 OSL Properties of Al_2O_3:C

Many materials have been studied and characterised in order to investigate their suitability to be used as an OSL dosimeter (Yoshimura & Yukihara, 2006). Aluminium oxide with carbon doping (Al_2O_3:C) is currently the most common substance in use although there are other materials being tested (Fatima et al., 2012).

The pure crystal structure of Al_2O_3 contains closely packed Al^{3+} and O^{2-} ions arranged in C_2 symmetry where four Al^{3+} ions surround an O^{2-} ion (Botter-Jensen et al., 2010). Al_2O_3 possesses an amphoteric nature that can react with both acids and bases and strong ionic inter-atomic bonding as well as high optical, thermal and chemical stability under irradiation (Hu, 2010). The crystal is unstable and sensitive to radiation, and functions as a catalyst in the formation of oxygen vacancy centre (Akselrod et al., 1993).

The aluminium oxide carbon doped material was a great choice for the OSLD because of its high sensitivity and relatively ease of fabrication (Bøtter-Jensen & Murray, 2001; Reft, 2009b). The optically stimulated luminescence dosimeter improved passive dosimetry as it has some potential advantages over other types of dosimeters.

2.6 Application of Optically Stimulated Luminescence Dosimeter in Radiotherapy

Numerous studies were carried out using OSLD in radiotherapy, this is due to its capability in measuring dose in external beam therapy (Dunn et al., 2013; Jursinic, 2007b) and brachytherapy (Andersen et al., 2009).

Andersen C. E. *et al.* (2009) carried out a study using a dose verification system to measure the absorbed dose rate on the basis of radioluminescence and OSL from Al_2O_3:C crystals attached to optical fiber cables in remotely after-loaded brachytherapy. A study by Viamonte A. *et al.* (2008) found out that OSLD demonstrated good agreement with ionisation chamber and diode measurements carried out under the same conditions for measurement of percentage depth dose (PDD) curve for ^{60}Co gamma radiation using solid water, energy, field size and SSD dependences as well as the dose response relationship between 25 and 400 cGy and the decay of the response with time following irradiation.

The Al_2O_3:C crystal OSLD has also been used in estimating its potential use as a proton dosimeter (Edmund et al., 2007). Besides, the OSLD has been characterised not only under high-energy photon (Dunn et al., 2013; Jursinic, 2007b; Jursinic & Yahnke, 2011; Kerns et al., 2011; Yukihara et al., 2004), but the OSLD performance as a passive dosimetry has also been evaluated for electron beams in radiotherapy as well (Yukihara et al., 2008).

CHAPTER 3: MATERIALS AND EQUIPMENTS

3.0 Overview

This chapter provides a list of the materials used in this study, which includes CT scanners, linear accelerators, treatment planning systems, phantoms, dosimeters as well as readers and scanners. The characteristics for each material are also briefly presented.

3.1 CT scanners: Philips Brilliance CT 64 Big Bore

Both University of Malaya Medical Centre and Pantai Hospital Kuala Lumpur installed Philips Brilliance CT 64 Big Core CT scanner (Philips Healthcare, USA) as shown in Figure 3.1 (a) and (b), respectively. The CT scans were used to scan the phantoms using automatic setting of kV and mAs with slice thickness of 3 mm.

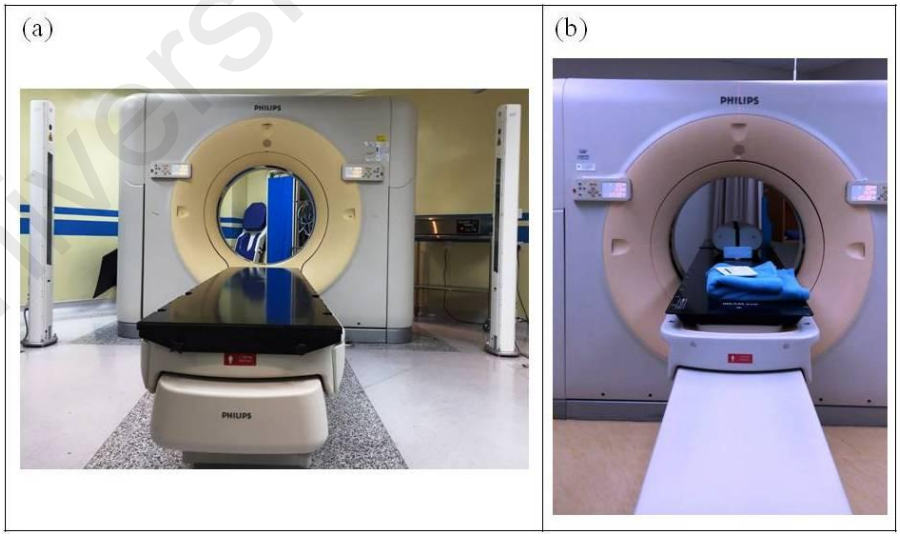

Figure 3.1: (a) CT scanners installed in UMMC and (b) Pantai Hospital Kuala Lumpur, respectively

3.2 Linear Accelerator

3.2.1 Varian Clinac 2100 C/D accelerator

A Varian Clinac 2100 C/D accelerator (Varian Medical System, Palo Alto, USA) as shown in Figure 3.2, was installed at the Clinical Oncology Unit, University Malaya Medical Centre (UMMC). All of the measurements for the characterisation of the OSLD, surface dose measurements and dose verification for 3D-CRT were carried out using the linear accelerator. The linear accelerator was kept under good service conditions, with a daily output variation of within 3%.

Figure 3.2: Linear accelerator Varian Clinac 2100 C/D installed in UMMC

3.2.2 Elekta Synergy linear accelerator

The verification of dose for IMRT and VMAT irradiations was carried out using the Elekta Synergy linear accelerator (Elekta, Maryland Heights, USA), as shown in Figure 3.3, which was installed in Pantai Hospital, Kuala Lumpur.

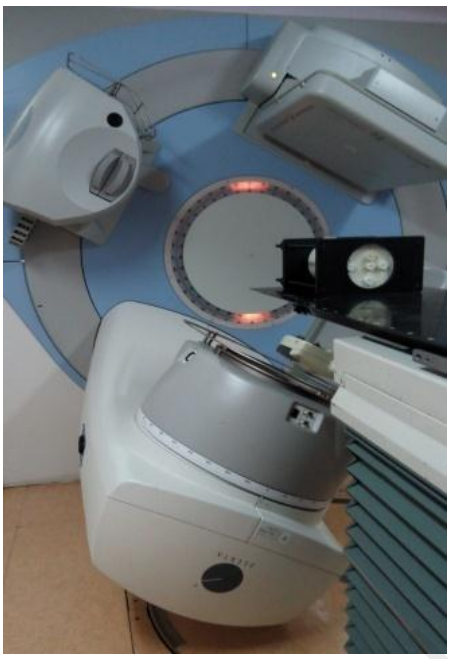

Figure 3.3: Elekta Synergy linear accelerator

3.3 Treatment Planning System (TPS)

3.3.1 Eclipse TPS

The treatment plans for surface dose measurements of breast radiotherapy and 3D-CRT irradiations were created using the Eclipse TPS Version 10.0 software application (Varian Medical System, Palo Alto, USA). The TPS uses a pencil beam convolution algorithm with a grid size of 2.5 mm x 2.5 mm.

3.3.2 XiO TPS

XiO TPS Version 4.7 (Elekta, Maryland Heights, USA) was used to formulate the plans for the IMRT irradiations. The TPS uses superposition calculation algorithms, and has a grid size of 2.0 mm × 2.0 mm.

3.3.3 Monaco TPS

Monaco TPS Version 3.20.01 (Elekta, Maryland Heights, USA) was used to formulate the plans for the VMAT irradiations. The TPS uses Monte Carlo calculation algorithm, and has a grid size of 2.0 × 2.0 mm^2.

3.4 Phantoms

3.4.1 OSLD jig

An OSLD jig with dimensions of 30 × 30 × 1 cm^2, together with an interchangeable slot to allow reproducible positioning of OSLDs as shown in Figure 3.4, were fabricated using Perspex. Schematic diagram of the jig can be found in APPENDIX A.

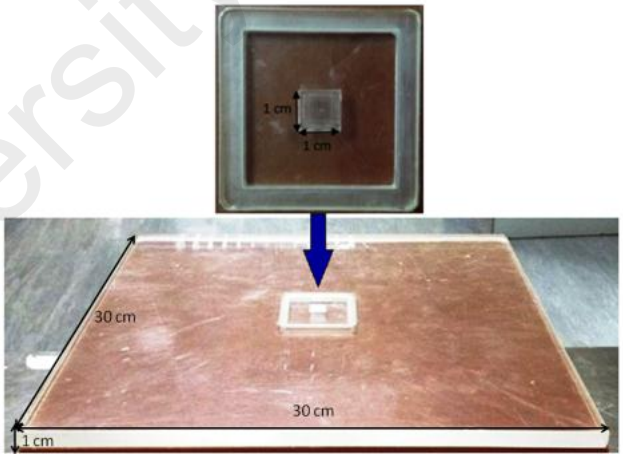

Figure 3.4: The OSLD jig

3.4.2 Solid water phantom

Solid water phantom (Gammex, Middleton, USA) with dimensions of 30 × 30 × 20 cm^3 as shown in Figure 3.5, was used to provide sufficient phantom scattering during measurement.

Figure 3.5: Compilation of solid water phantoms

3.4.3 Cylindrical IMRT head and neck phantom

A cylindrical IMRT head and neck phantom (model 002HN, CIRS Tissue Stimulation and Phantom Technology, USA) with a diameter of 16 cm and a length of 30 cm as shown in Figure 3.6 was used to carry out the angular dependence and dose verification works. The phantom consists of a fabricated OSLD holder rod with a diameter of 1.27 cm and a length of 15 cm.

Figure 3.6: The cylindrical IMRT head and neck phantom (model 002HN, CIRS)

3.4.4 Atom anthropomorphic phantom

The anthropomorphic phantom used was an Atom adult anthropomorphic phantom model 702-G (CIRS Tissue Stimulation and Phantom Technology, USA), as shown in Figure 3.7. The sections of the upper body and the pelvis were used in the study of surface dose measurement and dose verification, respectively. The phantom has OSLD slots positioned in various organs throughout the phantom. For the upper body section, the phantom has removable breasts that can be used to simulate the chest wall and breast of the patients. The pelvic part of the Atom anthropomorphic phantom was used in pelvis irradiation simulating prostate radiotherapy.

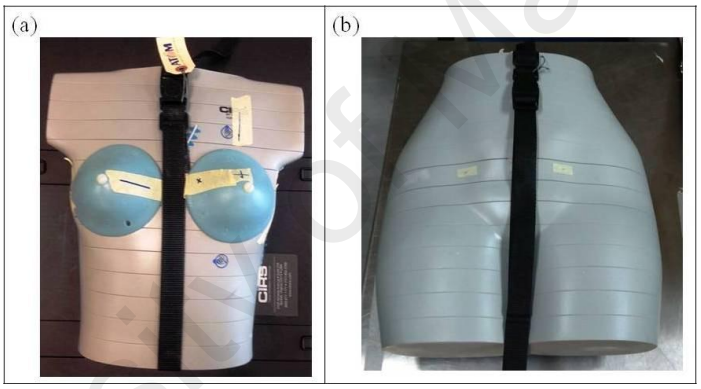

Figure 3.7: (a) Upper body and (b) pelvic section of Atom anthropomorphic phantom, respectively

3.5 Dosimeters

3.5.1 Markus ionisation chamber

A parallel-plate ionisation chamber (Markus type 23343 parallel plate ionisation chamber, PTW Freiberg, Germany) as shown in Figure 3.8 was used in measuring the

percentage depth dose (PDD) of the build-up region. The specifications of the Markus ionisation chamber are summarised in Table 3.1.

Figure 3.8: Markus ionisation chamber

Table 3.2: The specification of parallel plate ionisation chamber (Chen et al., 2010)

Parameters	**PTW original Markus**		
	Wall	**Collecting electrode**	**Window**
Material	Polymethylmethacrylate	Graphite PMMA	Polyethylene (CH_2)
Density	1.189 g/cm^3	1.189 g/cm^3	0.930 g/cm^3
Diameter (w)	6 mm	5.3 mm	-
Separation (s)	0.35 mm	2 mm	-
Thickness	-	-	2.5 mg/cm^2

3.5.2 Gafchromic EBT3 film

Gafchromic EBT3 Films (ISP, New Jersey, USA), as shown in Figure 3.9, were used as a comparison against the OSLD readings obtained in this research. The film is structurally symmetrical, and has three active substrate layers (30 microns) sandwiched with clear polyester layers (125 microns). The films were cut into pieces of 2 × 2 cm^2. The film was marked at the edge with a marker in order to identify film orientation during the scanning process (Butson et al., 2006). The films were scanned 24 hours after irradiation using a flat bed scanner (Epson Expression 1000XL flatbed scanner).

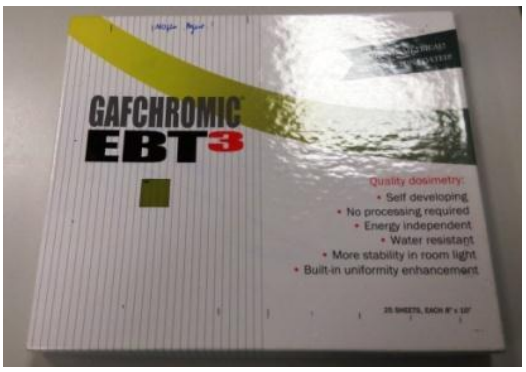

Figure 3.9: Gafchromic EBT3 film

3.5.3 Optically stimulated luminescence dosimeter (OSLD)

The OSLD used were nanoDot dosimeters (Landauer, Inc., Glenwood, IL) with a 5 mm diameter disc which is aluminium oxide carbon doped (Al_2O_3:C) sensitive area encased in light tight 1 × 1 × 0.2 cm^3 plastic carriers. The dosimeter, as shown in Figure 3.10 has a density of 1.03 g/cm^3. Each of the nanoDots has an alphanumeric sensitivity code and a serial number which provide the sensitivity information of the dosimeter. On the other side of the nanoDot is a 2D barcode that contains a user-friendly serial number to make the recording and tracking processes easier.

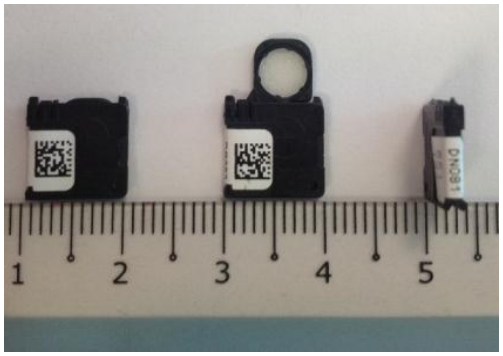

Figure 3.10: The nanoDot OSLD

3.6 Reader and scanner

3.6.1 MicroStar Reader system

The OSLDs were read using a MicroStar Reader (Landauer, Inc., Glenwood, IL). The reader, as shown in Figure 3.11, needs to be warmed up for at least 10 minutes before the readout process to stabilise and erase the residual signal from previous readout sessions. There are two available readout modes, which are low dose calibration and high dose calibration. For the low dose calibration mode, the maximum stimulation intensity is used to produce a high OSL signal at a low dose with a readout depletion of the OSL signal in the range of 0.2–0.3%. The high dose calibration mode was chose in this characterisation work in which the reader used a lower stimulation intensity; the readout depletion was less than 0.1% (IAEA, 2013).

The variations in the reader's sensitivity were checked prior to every reading process, including checking the background signal, photomultiplier tube (PMT) counts from the C-14 source , and counts from the PMT with the shutter open and the LEDs on to indicate beam intensity. The readout process of the nanoDot was initiated by scanning the barcode, and then mounting it into a cassette placed in the reader's drawer. During the readout, the electrons trapped in the sensitive materials are stimulated by an array of 36 green lights, and the blue light emitted by the OSL materials is detected and measured by a photomultiplier tube. In this study, the MicroStar Version 4.3 software application was used in order to display and export the data in Microsoft Excel format for further analysis. The actual reading of the OSLD, which corresponded to the dose delivered, was achieved by subtracting the readout of post-irradiation with the readout of pre-irradiation. In this study, the OSLDs were pre-irradiated with 50 cGy in order to have a consistent mode for the OSLD readout.

Figure 3.11: The MicroStar reader system which consists of a loader, a barcode scanner and a laptop

3.6.2 Epson Expression 1000XL flatbed scanner

An Epson Expression 10000XL flatbed scanner (Epson America, Inc. Long Beach, CA) as shown in Figure 3.12, was used to scan the films. By using transmission mode, with a resolution and format set to 96 dots per inch (dpi) and 48-bits RGB format, respectively, the images were saved in TIFF format to avoid compression and loss of data. The images were analysed using the ImageJ 1.47 software application (National Institute of Health, USA).

Figure 3.12: Epson Expression 1000XL flatbed scanner

CHAPTER 4: DOSIMETRIC CHARACTERISATION OF OPTICALLY STIMULATED LUMINESCENCE DOSIMETER (OSLD) UNDER MEGAVOLTAGE PHOTON ENERGY

4.1 Overview

In radiotherapy, different parameters were used in treating patients who differed in size and location of target areas. An exact knowledge of the dose received by the target area as well as surrounding organs are important in preventing insufficient or excessive dose been delivered. As OSLD is a relatively new dosimeter, characterisation work need to be done in order to assess the physical characteristics and responses of the dosimeters to function as a radiation dosimeter under megavoltage energy. Basically, an ideal dosimeter should possess at least one physical effect that is a function of the measured dosimetric quantity and can be used for radiation dosimetry with proper calibration.

In this study, the desirable dosimeter properties of OSLD will be characterised specifically on the calibration, linearity, reproducibility, energy dependence, repetition rate dependence, field size dependence, source to surface distance (SSD) dependence, fading effect, signal depletion per readout, sensitivity of the dosimeter towards multi exposure of irradiation and angular dependence.

4.2 Methodology

4.2.1 Calibration, Linearity and Reproducibility Measurement

The OSLD were irradiated using a 6 MV photon beam under standard conditions of 1.5 cm depth, 100 cm SSD and 10 × 10 cm^2 field size using 30 × 30 × 20 cm^3 solid water phantoms as shown in Figure 4.1. This setup is henceforth called the "standard setup".

The OSLD was calibrated under different doses from 10 cGy up to 1000 cGy for 6 MV and 10 MV photon beams. The irradiations were repeated three times by placing the dosimeter at d_{max} (1.5 cm for 6 MV, 2.5 cm for 10 MV), perpendicular to the central beam axis. The calibration was carried out objectively to obtain the calibration equations in order to convert OSLD count to dose in unit cGy.

The linearity of nanoDot OSLD was carried out to investigate the relationship of OSLD response with different delivered dose. The irradiations were repeated three times by placing the dosimeter perpendicular to the central beam axis.

A reproducibility test was carried out to investigate the ability of OSLD to reproduce the same reading throughout three rounds of measurements. It was determined based on the average standard deviation of the repeated measurements in the linearity test.

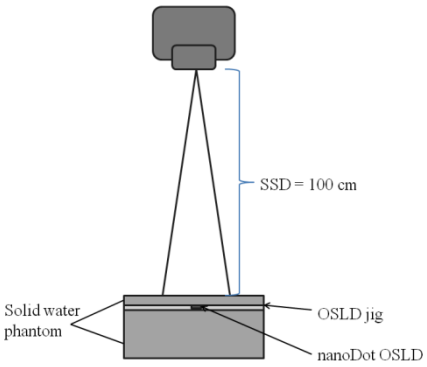

Figure 4.1: The standard setup used in measurement of calibration curve, linearity and reproducibility studies

4.2.2 Energy Dependence Measurement

The energy dependence study aims to investigate the response of the OSLD towards different energy photon beams. The OSLD was irradiated using the standard setup under 6 MV photon and 10 MV photon beams. The measured reading by OSLD under 6 MV and 10 MV photon beams was then converted to dose using the 6 MV calibration curve as mentioned in Section 4.2.1. The energy dependence was evaluated based on the difference in the dose obtained when irradiated using two different photon energies.

4.2.3 Repetition Rate Dependence Measurement

The repetition rate dependence study was carried out to investigate the response of OSLD towards various repetition rates. By using the standard setup, the OSLDs were irradiated using a 100 MU/min dose rate, up until 600 MU/min. The responses of OSLDs were then normalised to delivered dose of 200 MU.

4.2.4 Field Size Dependence Measurement

The objective of field size dependence study was to identify the relationship of OSLD responses with various field sizes used. By using the standard setup, the OSLDs were exposed to 200 MU using an energy and dose rate of 6MV and 600 MU/min respectively. The field size dependence was identified by varying field sizes ranged from 5 × 5 cm^2 to 30 × 30 cm^2 with increments of 5 × 5 cm^2. The OSLDs response for each field size was normalised to a response with a field size of 10 × 10 cm^2 and then compared to the output factor of the linear accelerator.

4.2.5 Source to Surface Distance Dependence Measurement

The source to surface distance (SSD) dependence of OSLD was carried out to investigate the response of OSLD towards the various SSDs employed. The study was carried out by exposing the OSLD to a 200 MU dose using the standard set up with varying SSDs ranged from 80 cm to 140 cm with 10 cm increments. The response of the OSLD was compared to the doses calculated based on inverse square law.

4.2.6 Signal Fading Characteristics of OSLD Measurement

The OSLDs were irradiated with 200 MU using the standard setup. The OSLDs were read out one minute after irradiation and then every 3 minutes for the first 15 minutes. After the initial transient signal decay period, the OSLDs were read out every half hour for four hours without erasing the previous signal.

4.2.7 Signal Depletion per Readout Measurement

The signal depletion per readout of a nanoDot OSLD was investigated by exposing the OSLD to 200 MU using the standard setup. The OSLD was then repeatedly read 200 times after a period of one day post-irradiation. The reading process involved opening the reader draw, closing it, and then initiating a read with no time delay in between readings. The depletion of the OSLD's signal per readout was determined by normalising the average OSLD's response over the initial reading. The total time taken for the reading process was approximately one and a half hours during which the fading was considered negligible.

4.2.8 Effect of Cumulative Dose Measurement

The OSLDs was irradiated with a 6 MV energy beam using the standard set up and 2 Gy dose were delivered at a time. The irradiations were repeated for until the dose accumulated was 20 Gy. The OSLDs were read using a MicroStar Reader after each exposure. The response of the nanoDot OSLD was correlated to the accumulated delivered dose.

4.2.9 Angular Dependence Measurement

The angular dependence study was carried out to investigate the OSLD response towards various incident beam angles and OSLD orientations. By using a cylindrical IMRT head and neck phantom (refer to Section 3.4.3), the OSLD was placed in a slot with an interchangeable rod. The slot was positioned at the centre of the phantom. Using the standard setup, the gantry angle was set at 0°. 200 MU was delivered to the nanoDot

OSLD. The angular dependence of the nanoDot OSLD was investigated by rotating the OSLD from 0° to 360° with 30° increments for the x- and y- axis of the dosimeter. The rotating orientations of OSLD are shown Figure 4.2. The measurements for each angle were repeated twice.

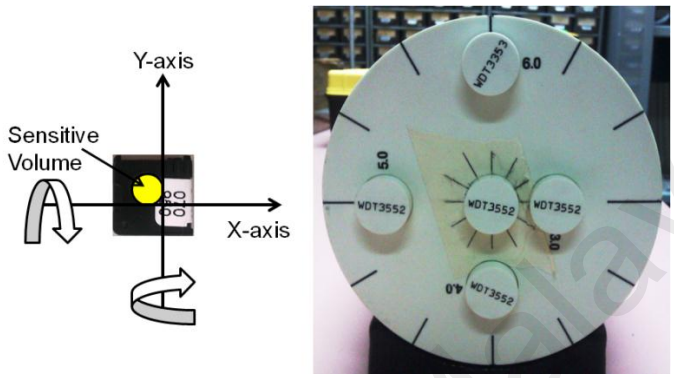

Figure 4.2: The x-axis and y-axis rotating orientation of OSLD in measuring the angular dependence

4.3 Results and Discussion

4.3.1 Calibration Equations, Linearity and Reproducibility

The calibration curves for the 6 and 10 MV photon beams (Figures 4.3 and 4.4, respectively) were established using Microsoft Excel 2007 (Microsoft, 2007) by applying a polynomial 2nd degree trendline for high dose irradiations, as recommended by the OSLD manufacturer (Landauer, 2012) and previous studies (Perks et al., 2008). This was due to the non-linear response of the OSLD to the increase of dose in the megavoltage energy. The calibration equations for both 6 MV (Eq. 4.1) and 10 MV (Eq. 4.2) photon beams were henceforth used in converting the counts to the absorbed dose of the OSLD.

$$D = -6 \times 10^{10} a^2 + 2.2 \times 10^{-3} a + 2.89 \text{.....Eq 4.1}$$

$$D = -6 \times 10^{10} a^2 + 2.2 \times 10^{-3} a + 4.17 \text{.....Eq 4.2}$$

where D is the measured dose in cGy, and a is the measured count by OSLD.

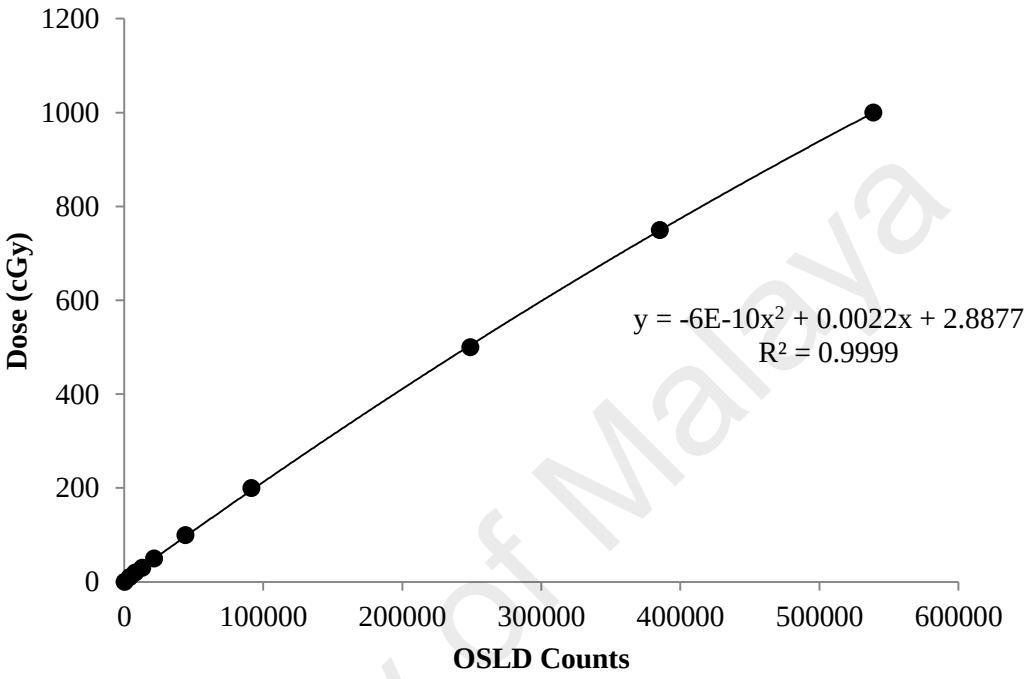

Figure 4.3: The calibration curve for 6 MV photon beam

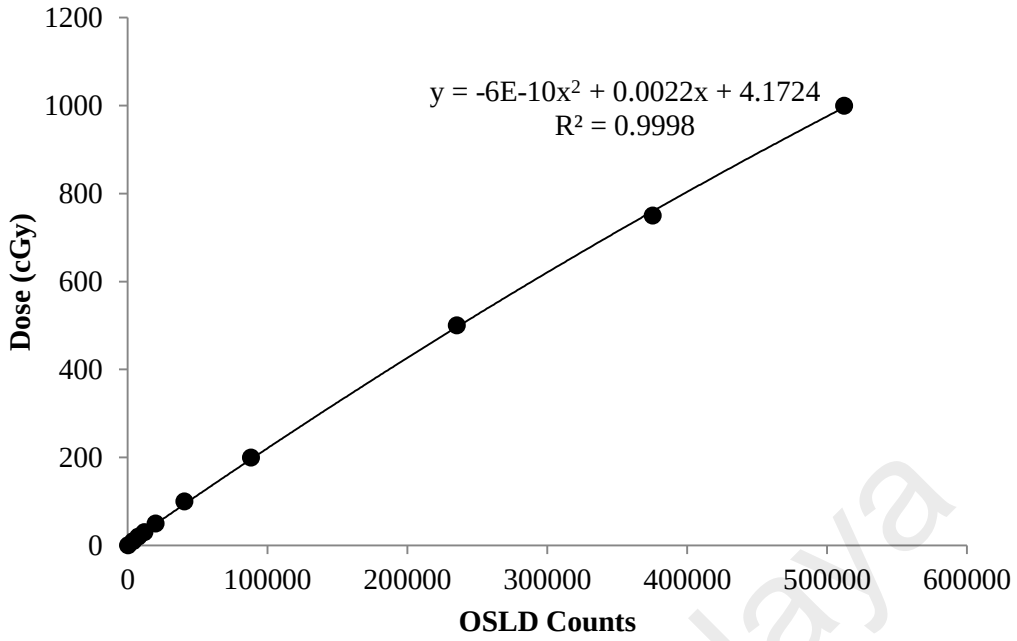

Figure 4.4: The calibration curve for 10 MV photon beam

The linearity for the 6 and 10 MV photon beams were then measured and the graphs are as shown in Figure 4.5. The linear regression coefficient resulted in R^2 values of 1.00 and 0.99 for the 6 and 10 MV photon beams, respectively. The graphs have shown good polynomial 2nd degree correlations since the line through the points on the graph fits the trend of the data. Despite the excellent linearity, previous studies have demonstrated that the OSLD response was linear from 1 cGy to 300 cGy (Dunn et al., 2013; Jursinic, 2007b) and behaved supra-linearly for a dose exceeding 300cGy (Jursinic 2010).

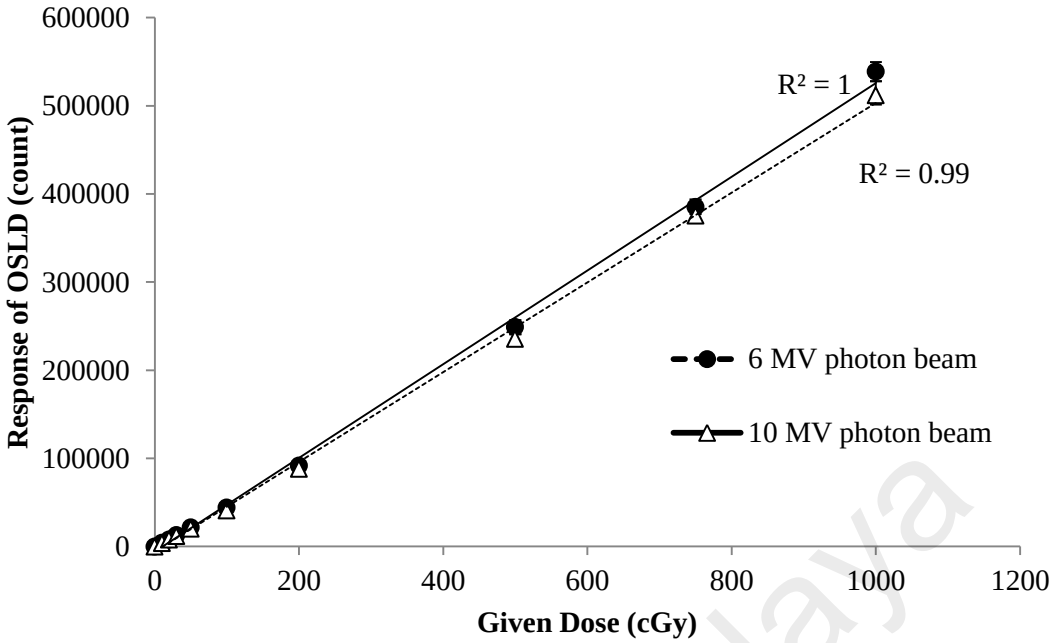

Figure 4.5: Linearity of OSLD for 6 MV and 10 MV photon beam

The reproducibility of the OSLD was determined based on the average standard deviation of the repeated measurements at different dose levels. In this study, the OSLD showed a good average reproducibility of 99.93% and 99.84% for 6 and 10 MV photon beams, respectively.

4.3.2 Energy Dependence

The energy dependence of the OSLD was investigated under 6 and 10 MV photon beams. In this study, the responses of the OSLD, which measured in count, were converted to dose using the respective energy calibration equation (Eq.4.1 and Eq. 4.2) and were subsequently compared with each other by plotting the graphs together as illustrated in Figure 4.6. The average deviation energy dependence between 6 MV and 10 MV was found to be within 5.23%.

The result was slightly different from the results of the study by Schembri *et al.* (2007) where the response for 6 MV and 18 MV photon beams differed by 4%. The study by Yukihara *et al.* (2008) found that the beam energy dependence for the 18 MV photon beam was 0.51% of the response for the 6 MV photon beam (Yukihara et al., 2008). Jursinic (2007) reported no dependence of radiation energy for the 6 and 15 MV x-rays, and there was little energy dependence found by Dunn *et al.* (2013) for over the clinical range.

Generally, the energy dependency of a dosimeter was related to the stopping power and the atomic number of its material. Various materials have different atomic numbers and a high atomic number will result in a high stopping power (Northcliffe & Schilling, 1970; Ziegler, 2013).

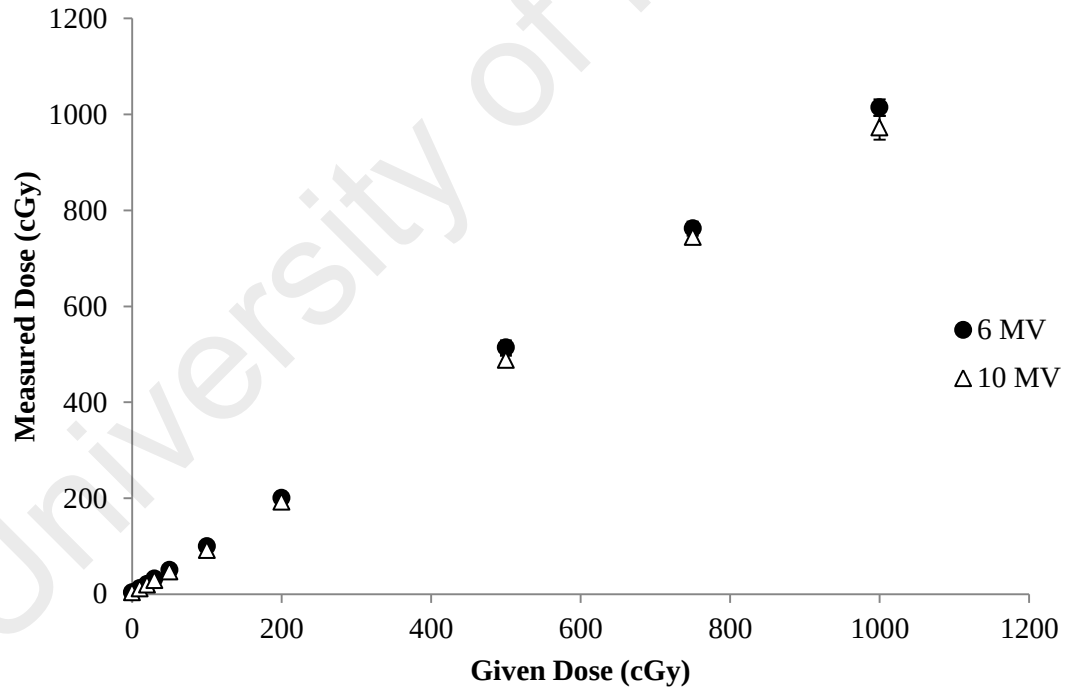

Figure 4.6: The measured dose of OSLD for 6 MV and 10 MV photon beams calibrated using 6 MV equation

4.3.3 Repetition Rate Dependence

The repetition rate dependence of OSLD towards the linear accelerator repetition rate was investigated and the OSLD responses were normalised to the delivered dose of 200 cGy as illustrated in Figure 4.7.

In this experiment, the maximum deviation was found to be -2.60% at dose rate of 200 MU/min. The average dependence for all dose rates was -0.30%. The result differed from previous the results in the study by Jursinic (2007) which found that no dose-per-pulse dependence over a 388-fold range.

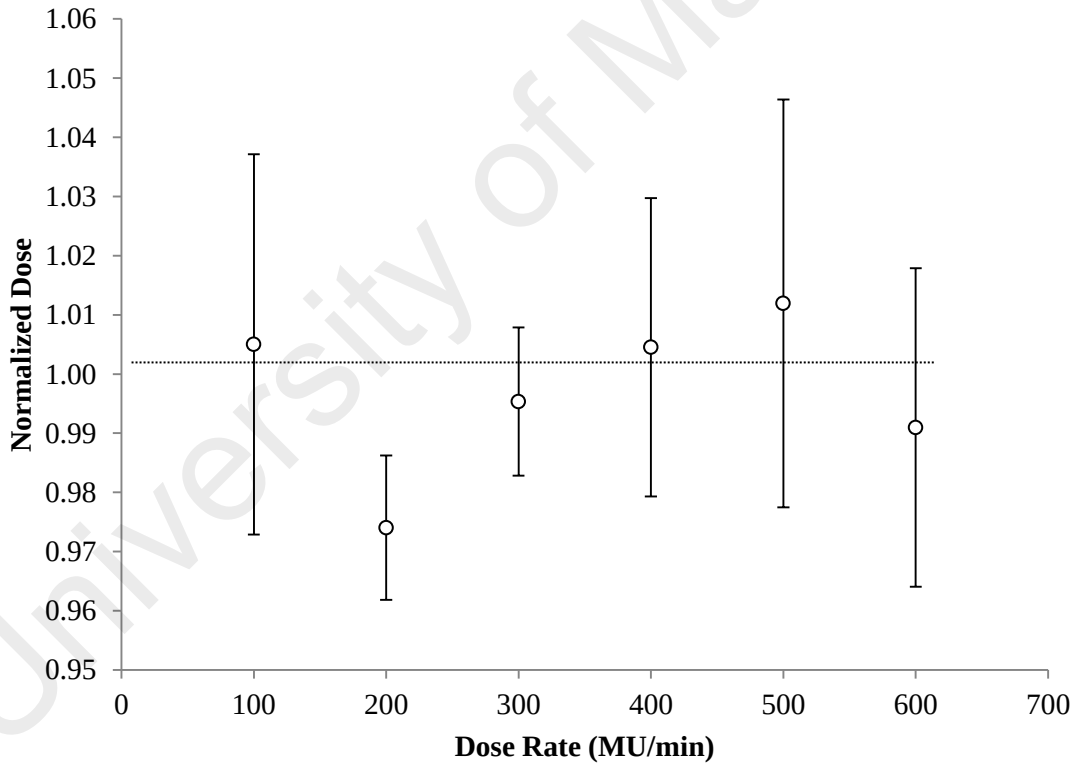

Figure 4.7: The response of the OSLD towards different dose rate

4.3.4 Field Size Dependence

In the investigation of the response of the OSLD to various field sizes, the doses recorded were normalised to the standard output factor of the linear accelerator for respective field sizes. According to Figure 4.8, the maximum percentage difference recorded was 3.81% for field size of 5 × 5 cm^2 to 20 × 20 cm^2, and the percentage difference recorded was higher for field size larger than 20 × 20 cm^2. The percentage difference was 9.13% at 30 × 30 cm^2 field size. This is due to the enhanced effect of OSLD as well as the increase in scatter component of the beam in a larger field size. The results differed from the study by Yukihara *et al.* (2008), which recorded that the maximum discrepancy observed was within 1%. This may be due to the difference in the set up and materials used in their study, in which they compared the dose measured by OSLD with the ionisation chamber.

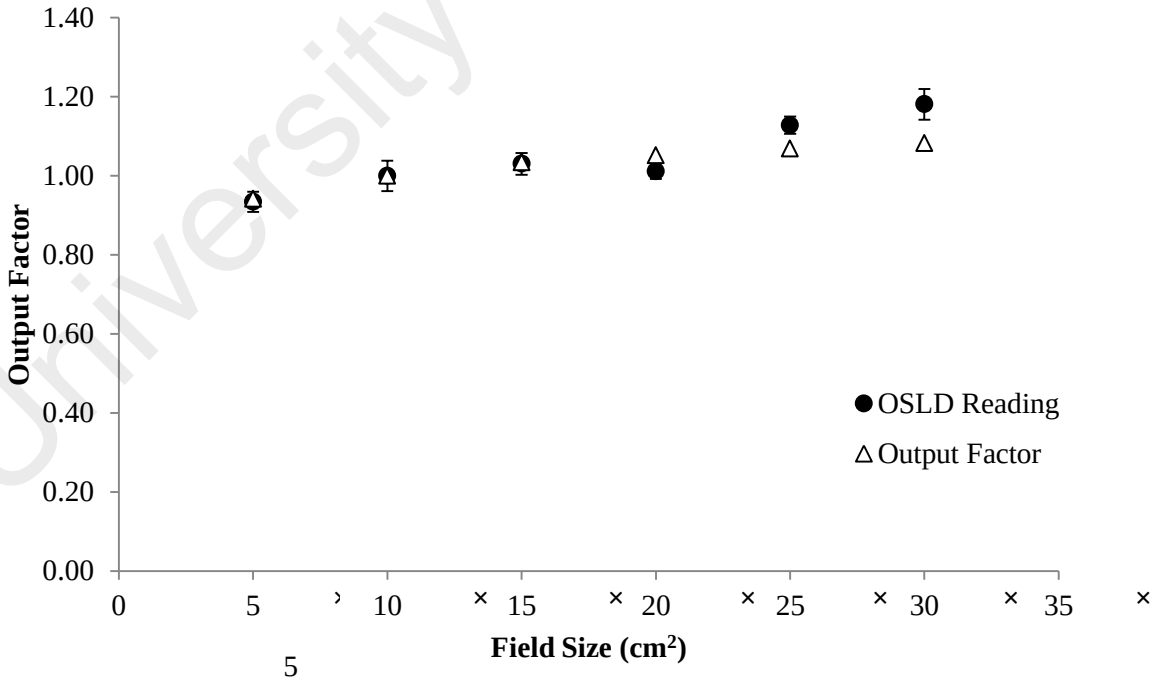

Figure 4.8: Normalised dose of OSLD responses to the standard output factor of the linear accelerator for respective field sizes

4.3.5 SSD Dependence

The measured dose of the SSD from 80 cm to 140 cm was compared to doses calculated based on the inverse square law. The calculated dose is the product of the inverse correction and the measured dose of 100 cm SSD. As illustrated in Figure 4.9, dose recorded by OSLD decreases when the SSD is increased mainly due to the inverse square law. The percentage of deviation between the measured dose and the calculated dose was within 2.34%.

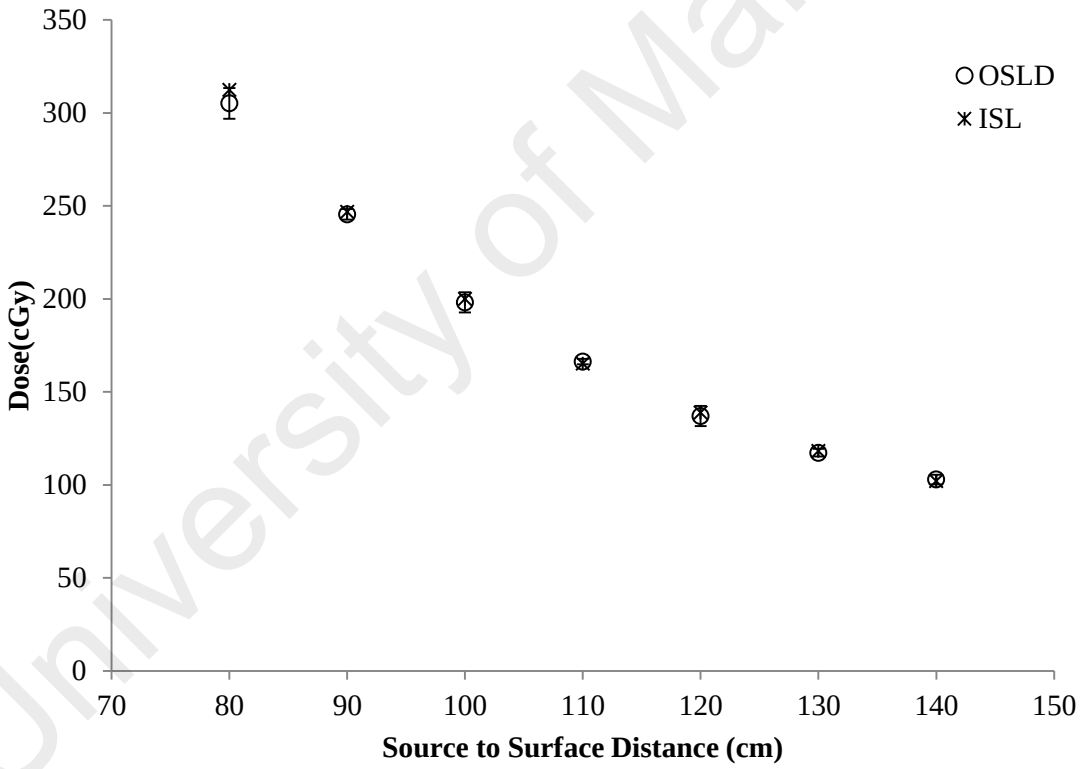

Figure 4.9: The comparison of dose recorded by the OSLD and the calculated dose using inverse square law

4.3.6 Signal Fading Characteristics of OSLD

The fading of the reading of the OSLD was studied and the measurements of the normalised dose to the 1 minute post-irradiation dose are shown in Figure 4.10. Within the first nine minutes of post-irradiation, the OSLD showed approximately 21.90% reduction as compared to the first signal. Meanwhile, after nine minutes, the OSLD showed a more stable response, with a deviation of only 1.26%. The OSLD showed initial rapid transient signal decay characteristic because of the unstable low level and non-dosimetric trap within the OSLD during the first nine minutes post-irradiation. Therefore, the OSLD requires time to enable the low level and non-dosimetric trap to stabilise (Yahnke, 2009). The result in this study is in agreement with the recommendation by IAEA which states that the OSLD should be read after 10 minutes post-irradiation due to the rapid fading during the first few minutes after irradiation (IAEA, 2013).

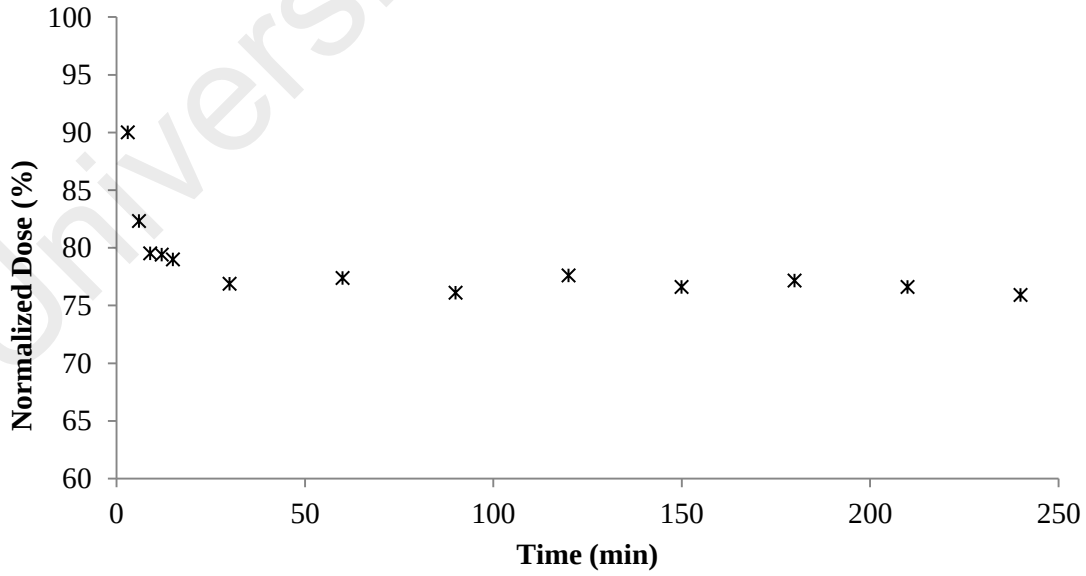

Figure 4.10: The percentage of normalised dose to the measured dose of 1 minute post-irradiation

4.3.7 Signal Depletion per Readout

A graph with the depletion magnitude for 200 repeated readouts is shown in Figure 4.11. The signal depletion of OSLD occurred with multiple readouts, as over 200 repeat readouts, the OSLD lost 8.47% of its original signal. Based on the linear trend line plotted, the data correlation which represented by the R^2 was 0.8868. The measured dose decreased by 0.06 cGy or about 0.03% per readout is in agreement with the study by Dunn *et al.* (2013) which recorded 0.03% decreased per readout over 190 readouts. A study by Jursinic (2007) found that the signal depletion of OSLD was 0.05% per readout for a total of 25 readouts.

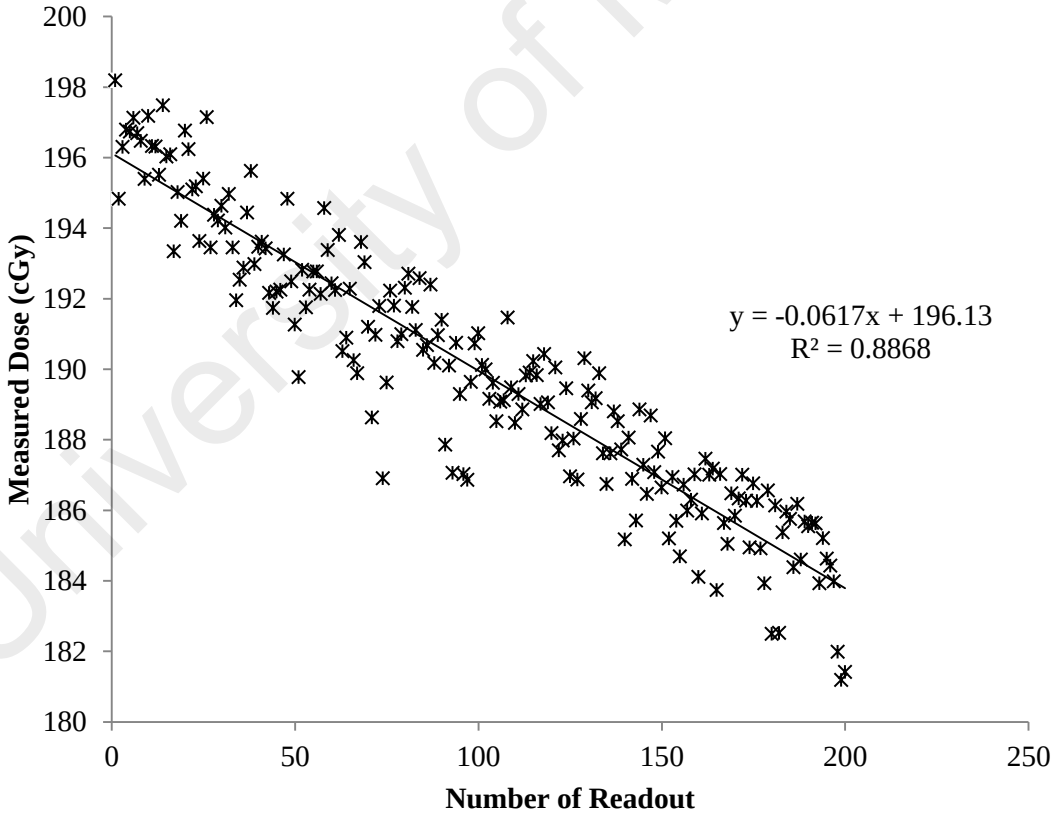

Figure 4.11: Signal depletion per readout of OSLD signals for 200 readouts

4.3.8 Sensitivity Towards Accumulated Dose

The sensitivity of the OSLD as a function of accumulated dose is illustrated in Figure 4.12. The accumulated dose of 20 Gy with 200 cGy intervals was given to the dosimeter. The sensitivity of every 200 cGy was determined as shown in Figure 4.12. The deviation of the sensitivity was found to be -4.38% within the accumulated dose of 10 Gy. This dropped after 10 Gy (fifth irradiation) with a maximum deviation of -49.80% at the accumulated dose of 20 Gy (tenth irradiation). This was due to the limitation in the calibration curve which was performed only up to 10 Gy.

In other studies, the sensitivity of the OSLD decreased by 4% per additional of 10Gy accumulated dose. The supra-linear response of the OSLD becomes more significant as the accumulated dose is increased (Dunn et al., 2013; Jursinic, 2007b, 2010).

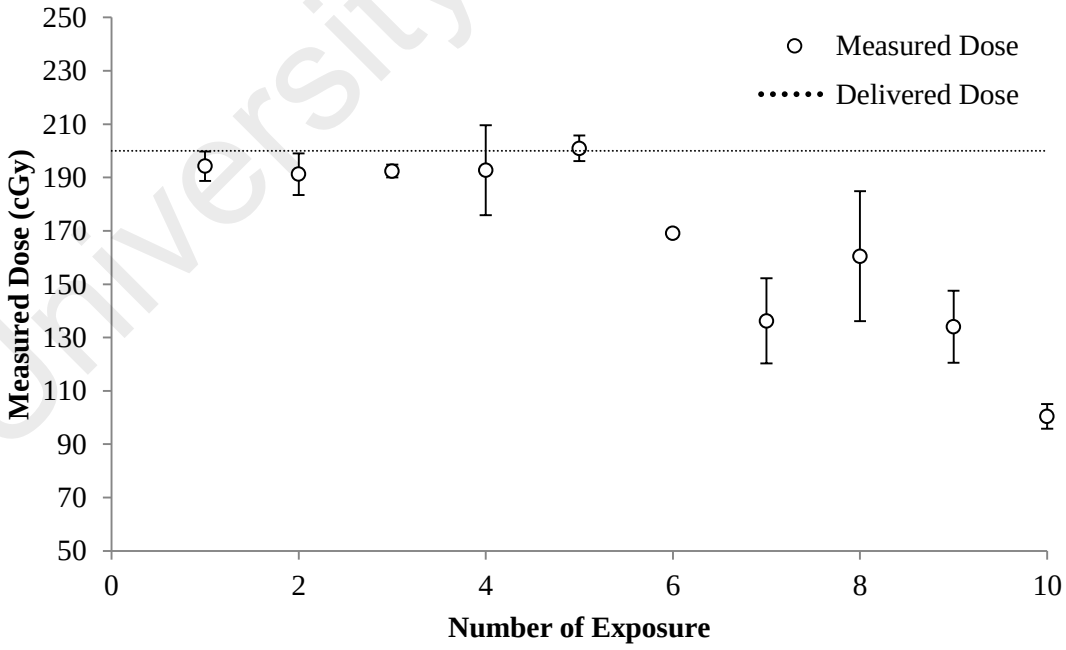

Figure 4.12: The sensitivity of OSLD towards the accumulated dose

4.3.9 Angular Dependence

Figure 4.13 shows the normalised dose of OSLD to the dose measured at 0 degree for the x- and y- axis rotating orientation. The maximum deviation for the x- and y- axis was 4.71% at rotating angle of 60° and 4.52% at a rotating angle of 330°, respectively. Overall, the average deviation for angles of the x-axis and y-axis rotation was 2.58% and 2.45%, respectively.

A previous study has reported that the angular dependence of the OSLD was less than 4% for the 6 MV photon beam (Kerns et al., 2011) and the uncertainty was 0.9% (Jursinic, 2007b). The OSLD showed the behavior of angular dependency because of the location of its sensitive volume which was not in asymmetric design. Thus, the difference in the buildup region during the irradiations led to the difference in the dose measured.

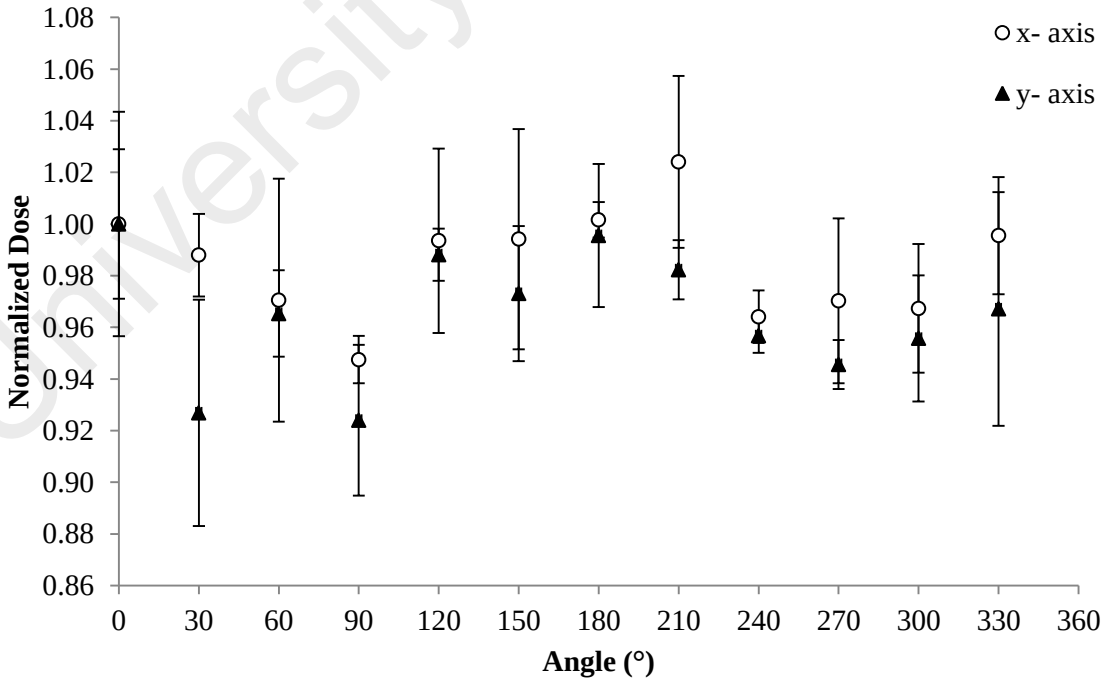

Figure 4.13: The normalised dose for each angle to the dose of 0 degree

4.3.10 Uncertainty Analysis

Table 4.1 shows a summary of the uncertainties of the OSLD's physical characteristics that had been determined throughout the characterisation works. The uncertainty of the linearity and reproducibility were chosen for only the 6 MV photon beam as the energy was usually used in clinical radiotherapy. The uncertainty for the field size was chosen to range from 5 x 5 cm^2 to 20 x 20 cm^2 based on the range of clinical radiotherapy.

After applying the quadrature summation of all the uncertainties, the overall uncertainty was 7.70%. However, if the OSLD was calibrated using either the 6 MV or 10 MV energy, the overall uncertainty would be 5.65%.

Table 4.1: The overall uncertainty of the physical characteristics of OSLD

Characteristics	Uncertainty, %	Remarks
Linearity	0.01	6 MV photon beam
Reproducibility	0.07	6 MV photon beam
Energy dependence	5.23	6 MV and 10 MV photon beams
Dose rate dependence	0.30	100 MU/min to 600 MU/min
Field size dependence	1.23	From 5 x 5 cm^2 to 20 x 20 cm^2
SSD dependence	0.65	80 cm to 140 cm
Signal fading characteristics	2.57	After 9 minutes
Signal depletion per readout	0.82	Up to 10 readouts
Sensitivity towards accumulated dose	2.84	Up to 10 Gy
Angular dependence (x-axis)	1.53	Average for all angles
Angular dependence (y-axis)	3.50	Average for all angles
TOTAL	**7.70**	Quadrature sum
	5.65	Without energy dependence

4.4 Conclusion

Based on the investigation of the physical characterisation of the OSLD for dosimetry under megavoltage photon beams, it can be summarised that: (1) the OSLD exhibits linearity of 100% and 99.99% for the 6 and 10 MV photon beams, respectively; (2) the OSLD demonstrated good reproducibility, with an average of 99.93% and 99.84% for the 6 and 10 MV photon beams, respectively; (3) the average deviation energy dependence between the 6 and 10 MV photon beams was found to be within 5.23%; (4) the dependency of the OSLD towards different dose rates was within 2.60%; (5) the OSLD showed 3.81% dependence in a field size of 5 x 5 cm^2 to 20 x 20 cm^2, which has increased as the field size increased; (6) the SSD dependence of the OSLD was found to be within 2.34%; (7) the OSLD showed a rapid transient signal decay for the first nine minutes post-irradiation, which gradually stabilised after this time, with a deviation of only 1.26%; (8) the signal of the OSLD decreased by 0.03% per readout, thus, it is recommended to take the few first readouts to determine the correct signal; (9) the sensitivity of the OSLD started to drop with an accumulated dose beyond 10 Gy; (10) the OSLD recorded an angular dependence of 1.53% and 3.50% for the x- and y-axis rotation respectively; and (11) the OSLD recorded an overall dependency of 5.04% without energy dependence.

As the OSLD exhibits a good response to function as a radiation dosimeter under megavoltage energy, it should possess a good reliability to be used in clinical and *in-vivo* measurements. The use of the OSLD in measuring surface dose is investigated in the next chapter.

CHAPTER 5: SURFACE DOSE MEASUREMENTS USING Al_2O_3:C OPTICALLY STIMULATED LUMINESCENCE DOSIMETER (OSLD) DURING RADIOTHERAPY

5.1 Overview

In previous chapter, it had been shown that OSLD demonstrated a good response towards megavoltage energy which is widely used in the external beam radiotherapy. In general, external beam radiotherapy (EBRT) is a treatment technique used mainly for the treatment of cancers using high energy ionising radiation. During radiotherapy, the skin is at risk of skin toxicity such as erythema, necrosis, desquamation, dermal lymphatic and basal-cell carcinoma (Chang-Claude et al., 2005; Cooper et al., 2004; Van Vloten et al., 1987). Thus, the measurement of surface dose is beneficial in providing better clinical management of potential acute skin reaction as in *in-vivo* measurements, with dosimeter placed on the surface of skin, the dose to a point inside the patient can be derived (Jursinic & Yahnke, 2011). In addition, it serves as a form of treatment verification to ensure correct dose is being delivered during radiotherapy.

Surface dose is defined as the dose deposited at the boundary between air and phantom (S Devic et al., 2006). It is contributed by scattered radiation from phantom, air and solid materials. Higher surface dose is deposited by increasing the oblique beam incidence and field size as well as usage of beam modifier devices such as bolus, tray and immobilisation device (Bilge et al., 2009; Hsu et al., 2008, Kry et al., 2012).

In this chapter, the application of OSLD for surface dose measurement had been investigated in three parts. First, the WED of the OSLD on a flat solid water phantom was first determined. This is followed by surface dose measurement on flat solid water phantom and anthropomorphic phantom. The feasibility and accuracy of OSLD for

clinical surface dose measurement was then conducted on a patient cohort undergoing breast radiotherapy.

The works presented in this chapter had been published in PLOS ONE journal, volume 10, issue 6, doi:10.1371/journal.pone.0128544.g004, with the title of 'On the Use of Optically Stimulated Luminescence Dosimeter for Surface Dose Measurement during Radiotherapy'.

5.2 Methodology

5.2.1 Water Equivalent Depth (WED) of Optically Stimulated Luminescence Dosimeter (OSLD) Measurement

By using 20 cm of solid water phantoms as backscatter, 10 pieces of OSLDs were irradiated with 200 cGy dose using 6 MV photon beam. The field size was set to 10×10 cm^2 at 100 cm SSD. The OSLD were irradiated one at a time by placing the dosimeter at the central axis of the beam on the surface of the solid water phantom.

Using the same set up, a parallel-plate Markus ionisation chamber (Markus type 23343 parallel plate ionisation chamber, PTW Freiberg, Germany) was also used to measure surface and buildup doses. Sheets of 30×30 cm^2 Gafchromic XR-RV2 film (International Specialty Products, Wayne, NJ) with water equivalent thickness (WET) of 0.032 cm was used as buildup material. The WED of the film was calculated as a physical thickness of the film piece scaled by physical density of water (1.0g/cm^3). Markus ionisation chamber measurements were corrected for temperature and pressure, polarity and recombination. Correction factors for over response were applied to the Markus ionisation chamber readings using formula by Gerbi and Khan (1990) as shown in Eq 5.1 and Eq 5.2:

$$P'(d,E) = P(d,E) - \xi(0,E)le^{\alpha(d/d_{max})} \quad (\%)\text{.....Eq 5.1}$$

$$\xi(0,E) = (-1.666 + 1.982\,IR) \times (C - 15.8) \quad (\%/mm)\text{.....Eq 5.2}$$

where P and P' are the corrected and uncorrected percentage depth dose in build up region respectively, ξ(0,E) is over response of the chamber in percent, at the surface of the phantom, l is the plate separation (2 mm for Markus PTW 23343), α is a constant with value 5.5, d is depth in phantom and d_{max} are 1.5 cm and 2.5 cm for 6 MV and 10 MV respectively. IR represents the ionisation ratio which is 0.664 and 0.732 for 6 MV and 10 MV respectively using the specific setup in this study and C is the sidewall-collector distance (0.35 mm for Markus PTW 23343). The calculated $\xi(0,E)$ are respectively 5.407 and 3.324 for 6 MV and 10 MV photon beams.

The WED of OSLD was investigated by comparing average surface dose of OSLD with percentage depth dose (PDD) measurements using Markus ionisation chamber.

5.2.2 Surface Dose Measurement Using Solid Water Phantom

Surface dose measurement was performed by using three different dosimeters namely the Markus ionisation chamber, EBT3 film and OSLD on a solid water phantom. The dosimeters were placed on a 30 cm × 30 cm × 20 cm solid water phantom, at the central axis of 10 cm × 10 cm radiation field with SSD of 100 cm as shown in Figure 5.1. A dose of 200 cGy was delivered to each dosimeter, one at a time for photon energies of 6 MV and 10 MV. The measurements were repeated twice for each dosimeter. Absorbed doses recorded by all dosimeters were normalised to the 100% dose at d_{max}.

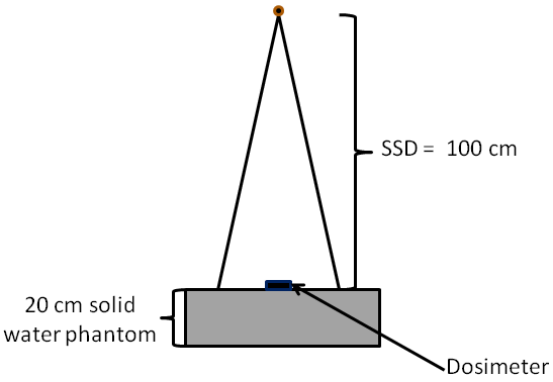

Figure 5.1: Set up used in surface dose measurement using solid water phantom

5.2.3 Effect of Beam Angle on Surface Dose

An OSLD was placed at the central axis on the surface of a 30 cm × 30 cm × 20 cm solid water phantom and irradiated using 6 MV photon beam under standard set-up (100 cm SSD and 10 cm × 10 cm field size) as shown in Figure 5.2. The OSLD response for different incident beam angles was evaluated by delivering a fixed number of MUs, with the linear accelerator gantry rotated to an angle. The incident beam angles of -75° to +75°, with increment of 15° were studied. The responses of the OSLDs were compared with EBT3 film measurements using the same experimental setup. The measurements were repeated twice for each dosimeter.

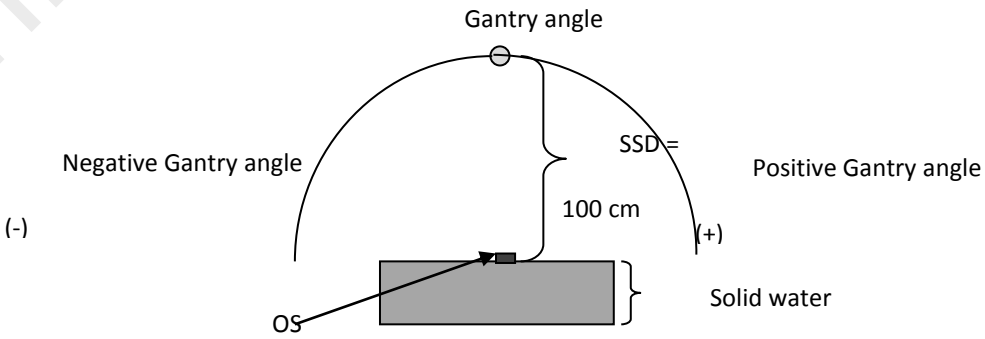

Figure 5.2: Rotation of the linear accelerator gantry

5.2.4 Surface Dose Measurement on Anthropomorphic Phantom

Prior to actual application of the OSLD on clinical patients, simulated breast radiotherapy treatments were carried out on an anthropomorphic phantom (Atom Phantom, CIRS, Norfolk, VA). Eclipse Treatment Planning System (TPS) (Varian Medical System, Palo Alto, USA) version 10.0 was used to create (i) a chest wall irradiation (with bolus) and (ii) a breast conserving (without bolus) radiotherapy treatment plans on CT images of the anthropomorphic phantom. The TPS used a pencil beam convolution (PBC) algorithm with a grid size of 2.5 mm x 2.5 mm. Two tangential opposed beams were used with different energy weighting and beam modifier devices such as the physical wedge. The chest wall surface dose measurements were carried out on the anthropomorphic phantom without breast attachment while breast conserving radiotherapy was carried out with breast attachment. During the measurement, the OSLDs were placed at 3 cm from the border of the medial and lateral beams (Hamers et al., 1991) as shown in Figure 5.3.

The contralateral dose was measured by placing the dosimeter on the tip of the nipple of the contralateral breast. The positions of the dosimeters were fixed by putting a marker on the surface for good reproducibility and accuracy. For chest wall measurements, the dosimeters were placed underneath the 1 cm thickness bolus. The response of the OSLD was compared with the measurements by EBT3 film and the dose predicted by Eclipse TPS. The measurements were repeated twice for each dosimeter. The isodose of the breast conserving using 6MV photon beam, breast conserving using 10MV photon beam, chest wall using 6MV photon beam and chest wall using 10MV photon beam plans are attached in APPENDIX B, APPENDIX C, APPENDIX C and APPENDIX D, respectively.

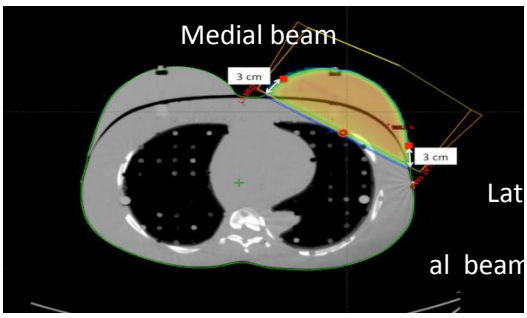

Figure 5.3: The placement of the dosimeters on the anthropomorphic phantom

5.2.5 Surface Dose Measurement: Patient Study

For surface dose measurement on patients, 5 patients undergoing breast conserving radiotherapy and 5 patients undergoing chest wall irradiation were recruited. The placement of the OSLD was the same as described in the anthropomorphic phantom study. Measurements were repeated at least twice during different treatment fractions throughout the whole course of breast radiotherapy. The OSLD measurements were also compared with EBT3 film measurements and TPS predicted dose.

A total dose of 40 Gy dose was prescribed for 15 fractions with a single prescribed dose of 2.67 Gy being delivered for each treatment fraction. The Planning Target Volume (PTV) coverage was planned to receive 95% to 107% of the prescribed dose (Jones, 1994). The OSLD measurements were compared with TPS predicted doses and EBT3 film measurements using paired sample t-test by IBM SPSS Statistics software for Windows (IBM SPSS, IBM, New York, USA) Version 21. The medical ethics was approval was given by the Medical Ethics Committee of University Malaya Medical Centre (UMMC) (Reference number: 1030.19). Written consent was waived, as the study did not involve the use of drugs and patient intervention. Verbal consent to the patient, a method approved by the medical ethics committee, was conducted before the radiotherapy treatment.

5.3 Results and Discussion

5.3.1 WED of OSLD Measurement

The WED of OSLD was determined by substituting the percentage of normalised surface dose to the dose at d_{max} measured by OSLD into the equation by the PDD graph of Markus ionisation chamber's measurements. The WED of OSLD was found to be 0.4 mm.

The OSLD with the intrinsic buildup of 0.4 mm consequently over-estimated the surface dose by 21.8 % for 6 MV photon beam. This means that OSLD is neither measuring surface dose at depth of 0 mm nor measuring skin dose at the depth of Hp (0.07) (Fry, 1992). ICRP defined skin dose which considered as the most radiosensitive layer at depth of 0.07 mm in the skin (Fry, 1992). However, anatomically, human skin consists of two layers which are the epidermis and dermis layers. The epidermis and dermis layers are physically 2.7 mm in thickness (Archambeau et al., 1995; Laurent et al., 2007). Thus, the OSLD which has WED of 0.4 mm can still be considered to measure dose to the skin layer, albeit at a greater depth than the basal skin layer.

5.3.2 Surface Dose Measurement Using Solid Water Phantom

Table 5.1: The comparison of the surface dose (normalised to 100% the dose at d_{max}) measured using Markus ionisation chamber, EBT3 film and OSLD for 6 MV and 10 MV photon beams.

Energy	**Mean Surface Dose ± 1 s.d (%)**		
	Markus	**EBT 3 Film**	**OSLD**
6 MV	15.95 ± 0.08	23.79 ± 0.68	37.77 ± 2.00
10 MV	12.64 ± 0.03	17.14 ± 1.68	25.38 ± 0.30

Table 5.1 shows the normalised response of the Markus ionisation chamber, EBT3 film and OSLD for 6 MV and 10 MV photon beams. The surface dose recorded for 6 MV photon measured by the detectors were higher than 10 MV photon due to the skin sparring effect of 10 MV photon. Markus ionisation chamber measured the lowest surface dose, followed by EBT3 film and OSLD. The differences between the three detectors are larger for the lower beam energy. This response is expected as the dose gradient in the buildup region for 6 MV photon beam is steeper than in 10 MV photon beam.

The measured WED and surface dose of Markus ionisation chamber, EBT3 film and OSLD in this study was compared to the measurements by Jong *et al.* (2014) which used MO*Skin* detector and EBT2 film. The relationship of the WED and surface dose are shown in Figure 5.4.

MO*Skin* detector and EBT2 film has WED of 0.070 mm (Kwan et al., 2008) and 0.122 mm, respectively (Jong et al., 2014). As for EBT3 film, which has low energy dependence and combined uncertainty (Sorriaux et al., 2013) has the active layer with density of 1.1 g/cm^3 and thickness of 17 µm. Structurally, the active layer was sandwiched between two layers of transparent polyester with thickness of 97 µm (S Devic et al., 2006) and the dosimeter has the intrinsic buildup of 0.16 mm. On the other

hand, the parallel-plate Markus ionisation chamber which has the entrance electrode window thickness scaled by the physical density of the electrode material, corresponded to the effective point at a depth (Chen et al., 2010) which is the water equivalent depth at surface. The WED of OSLD was found to be at 0.4 mm (refer to Section 5.3.1).

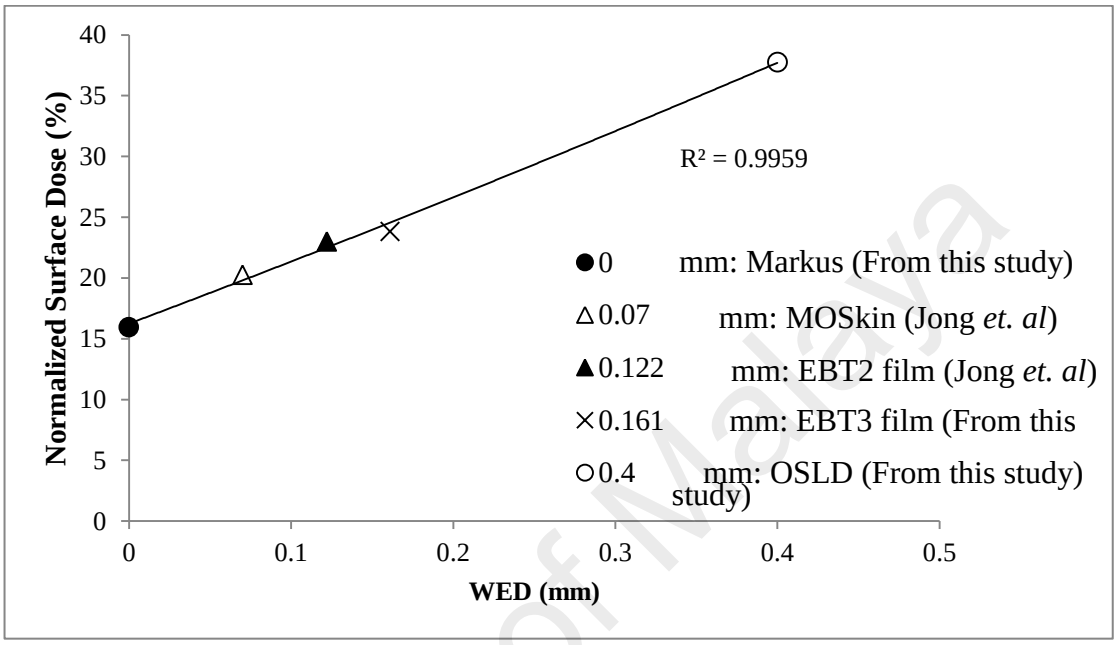

Figure 5.4: Normalised surface dose for dosimeters with different WED

The relationship between the WED and surface dose is shown in Figure 5.4. The data points were fitted in a simple linear trend line (R^2=0.996). An interpolation method was used to determine the correction factors of the OSLD for surface dose (Hp(0.0)) and skin dose (Hp(0.07)). *In-vivo* OSLD measurements can be used to predict surface dose (Hp(0.0)) and skin dose (Hp(0.07)) by means of applying a correction factor using the Eq. 5.3 and 5.4.

$$Surface\ dose, Hp(0.0) = D_{OSLD} \times 0.42 \quad \text{.....Eq. 5.3}$$

$$Skin\ dose, Hp(0.07) = D_{OSLD} \times 0.54 \quad \text{.....Eq 5.4}$$

Using OSLD measurements, it is possible to estimate the dose to the surface of the skin or the basal skin layer Hp(0.07) by means of a correction factor. However, one

should note that this correction factor can be applied for perpendicular beam incidence only.

Table 5.1 and Figure 5.4 indicate that the increase of WED which is the intrinsic buildup of the dosimeter, leading to the increase of measured surface dose. The increase of buildup which can be expressed in water equivalent depth led to the increase of dose measured as the effect of electrons attenuation and scattering with materials (Jong et al., 2014). It was shown by Devic *et al.* (2006) that the PDD increased from 14% at depth of 4 μm to 43% at a depth of 1 mm (S Devic et al., 2006).

5.3.3 Effect of Beam Angle on Surface Dose

Figure 5.5 shows the differences of surface dose measurements using OSLD which were normalised to the surface dose measurements using EBT3 film. The error bars represent 1 standard deviation (SD) of the mean of three repeated measurements. As the beam incident angle increases, the measured surface dose increased as a function of inversed cosine. For small incident beam angles ($\theta \leq 30^{o}$), the measured surface dose increased by less than 10%. At the maximum incident beam angles of 75^{o}, a 73% increase in the surface dose was found when measuring using OSLD. This may be due to the shift of the region of charged particle equilibrium toward the surface.

Compared to EBT3 film measurements, the dose recorded by the OSLD is higher with average percentage difference of 39.1 ± 17.5%. This is due to the different WED of the dosimeters. Both dosimeters showed a similar trend, showing an increase in the measured dose with increased incident beam angles. However, the EBT3 film measurements showed a steeper curve compared to the OSLD. This may be because of the slight angular dependence of the OSLD packaging design. Kern *et al.* (2011) measured the angular dependence of the nanoDot OSLD in a cylindrical phantom

(Kerns et al., 2011). They reported the angular dependence of the nanoDot detector to be <4%.

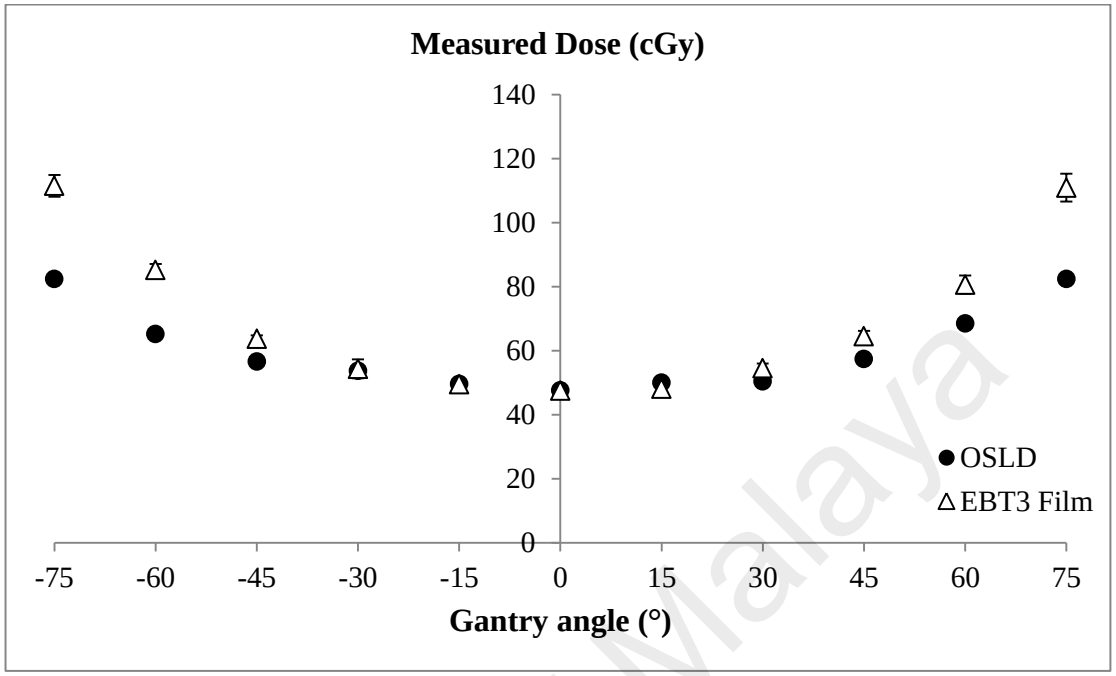

Figure 5.5: Differences of normalised surface dose of OSLD measurements to the EBT3 film's measurements

Oblique incident beam angles are expected to contribute to higher surface dose due to the shift of the charged particle equilibrium region to the surface and increase in electron contaminations and higher photon interactions within the phantom (Butson et al., 1996). All of these factors resulted in a combined effect of increased surface dose measured particularly during tangential breast radiotherapy treatments which the range of the gantry angle used was 49° to 58° positively or negatively from the y-axis.

5.3.4 Surface Dose Measurement on Anthropomorphic Phantom

Table 5.2: Surface dose measured using OSLD and EBT3 film for breast conserving and chest wall radiotherapy using 6 MV and 10 MV energies compared with the TPS predicted dose

Type of Irradiation	Energy	Dosimetry	Mean Surface Dose ± 1 SD (cGy)		
			Medial	Lateral	Contralateral
Breast Conserving	6 MV	TPS	137.0 ± 1.7	159.7 ± 2.6	4.4 ± 0.0
		EBT3	116.2 ± 1.0	123.7 ± 1.6	18.8 ± 0.6
		OSLD	138.0 ± 6.9	144.7 ± 3.3	22.2 ± 1.7
	10 MV	TPS	125.3 ± 1.9	131.8 ± 0.1	3.6 ± 0.0
		EBT3	113.0 ± 1.5	118.1 ± 1.3	20.2 ± 2.7
		OSLD	118.6 ± 0.6	131.9 ± 1.9	21.7 ± 0.9
Chest Wall	6 MV	TPS	273.4 ± 1.3	274.5 ± 0.0	2.8 ± 0.0
		EBT3	248.8 ± 2.4	247.4 ± 2.7	18.3 ± 0.1
		OSLD	265.1 ± 0.6	256.5 ± 2.4	19.0 ± 0.8
	10 MV	TPS	269.7 ± 0.2	259.8 ± 0.1	3.2 ± 0.0
		EBT3	251.4 ± 2.5	247.7 ± 1.5	21.0 ± 1.8
		OSLD	264.4 ± 3.0	254.0± 2.0	22.3± 0.5

Table 5.2 shows the surface dose measured on an anthropomorphic phantom. The OSLD and EBT3 film measurements were compared with TPS predicted dose. In general, OSLD recorded higher dose compared to EBT3 film for all exposures. The TPS appears to predict slightly higher dose for the treated breast while much lower dose were predicted for the contralateral breast.

For breast conserving radiotherapy, the average measured surface doses were found to range from 44.4% to 54.2% of the prescribed dose (267 cGy). Under 6 MV photon beam, OSLD measurements were higher than EBT3 by a factor of 1.19 and 1.17 for medial and lateral positions, respectively. The doses recorded from OSLD measurements were comparable to, or slightly lower than the TPS predicted doses. For the treatment plans delivered using 10 MV photon beams, the OSLD measurements

were also higher than the EBT3 film measurements, although by a lesser degree. The OSLD measurements were also comparable to the TPS predicted dose for this beam energy.

For chest wall radiotherapy, the average measured surface doses were found to range from 95.1% to 99.3% of the prescribed dose. The differences between the OSLD and EBT3 film measurements were also found to be smaller compared to breast conserving radiotherapy. For medial and lateral positions, the OSLD measurements were found to be higher than EBT3 film by a factor of 1.07 and 1.04, respectively for 6 MV photon beams. Using the same energy, the OSLD recorded lower surface dose as compared to the TPS predicted dose by a factor of 0.97 for medial position and 0.93 for lateral position. By using 10 MV photon beams, the OSLD measured a higher surface dose than EBT3 film for the medial and lateral positions of the treated breast, and a slightly lower dose as compared to the TPS predicted dose.

For surface dose of the contralateral breast, the OSLD and EBT3 film measurements were in close agreement with each other. However, large discrepancies were observed between the measurements and the TPS predicted dose values. The TPS predicted dose was less than 5 cGy for all measurement points whereas direct measurements showed that the actual surface dose to the contralateral breast could be more than 18 cGy. This represents 6.7% of the predicted dose.

In this study, small standard deviations reflected good reproducibility of the dosimeter's response and exposure setup. Based on the presented results, it had been showed that OSLD recorded higher surface dose as compared to EBT3 film responses for all positions in phantom and patient studies. This was due to the difference in WED of the dosimeters which OSLD has deeper WED as compared to EBT3.

TPS showed inconsistent measurements largely due to the variability in the points selected as skin surface on the TPS leading to large measurement uncertainty.

Other than that, the Eclipse TPS at this centre used PBC algorithm with a dose grid of 2.5 x 2.5 mm^2. The larger voxel size results in volume averaging effect. The inhomogeneity correction used by this algorithm is based on the equivalent tissue air ratio (ETAR) method, which has been found to have a less accurate dose prediction for air cavities and interfaces (Sim et al., 2013) as well as at the build-up region (Fraass et al., 1998). Skin sparing effect of 10 MV which lead to the higher dose recorded by 6 MV breast conserving radiotherapy compared to 10 MV for contralateral dose. Radiation dose to the contralateral breast are contributed by scattered radiations from collimator, wedge, and leakage and scatter from the primary radiation (Chougule, 2007; Wahba A. G. & Safwat, 2009). Monitoring of the dose to the contralateral breast is important as these low level radiation doses may induce secondary cancer (Brenner, 2010; Stovall et al., 2008; Yadav et al., 2008).

5.3.5 Surface Dose Measurement: Patient Study

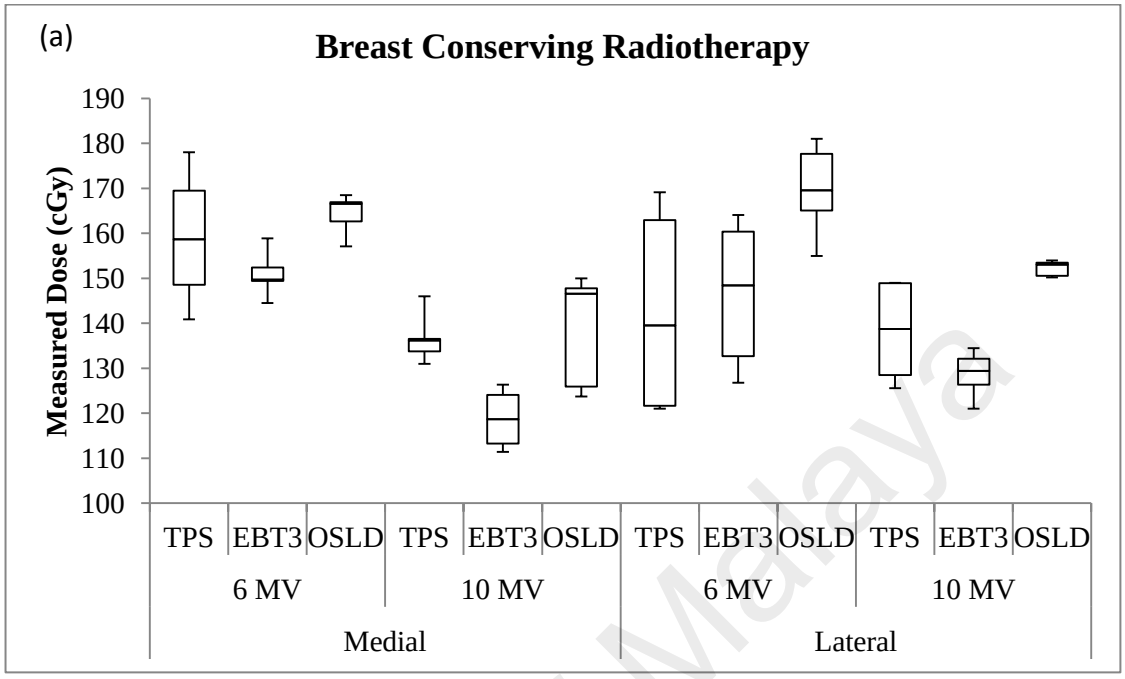

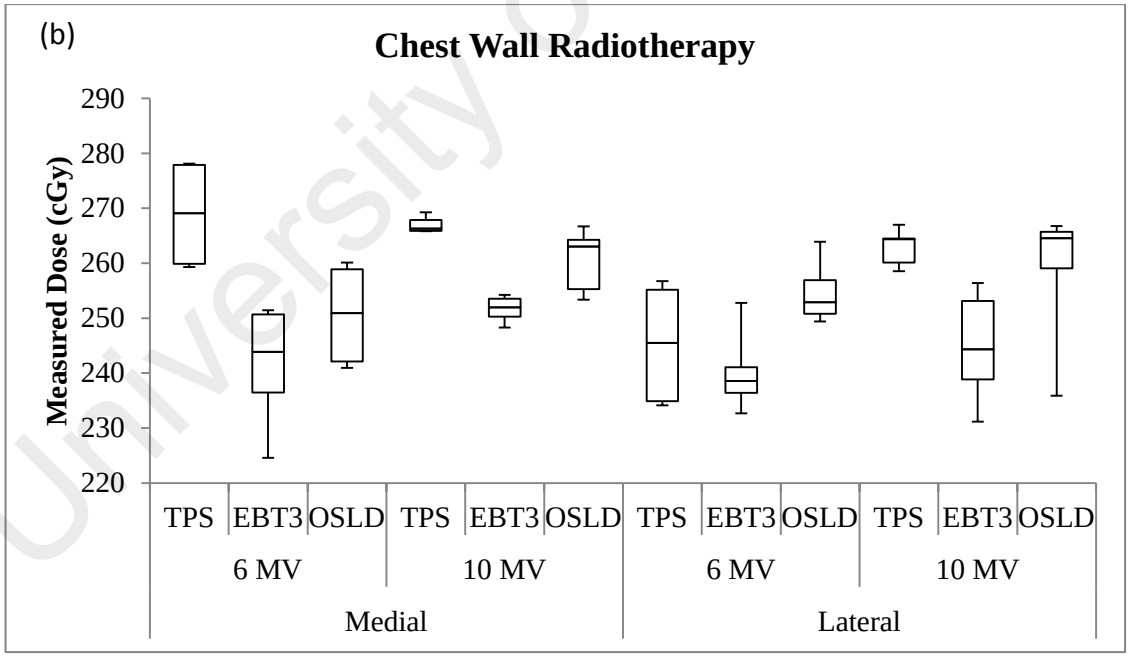

Figure 5.6: (a) Surface dose of the treated breast for medial and lateral positions during breast conserving and (b) chest wall radiotherapy, respectively

The *in-vivo* dose measurements of 5 breast conserving and 5 chest wall radiotherapy patients are shown in Figure 5.6 (a) and (b), respectively. Each box-plot represents the spread of 15 measurements (5 patients × 3 measurements). For breast conserving radiotherapy, the difference between the three measurements for the same patients was found to be ±7.71 cGy, ±4.14 cGy and ± 2.18 cGy for medial, lateral and contralateral positions, respectively. For chest wall radiotherapy, the differences were within ±7.11 cGy, 8.55 cGy and ±1.72 cGy for medial, lateral and contralateral positions, respectively.

The box-plots shows a similar trend for both breast conserving and chest wall radiotherapy, whereby the median doses measured by the OSLD were higher than those measured using EBT3 films. The small spread of the box-plots shows that the *in-vivo* measurements were quite consistent. However, day-to-day patient positioning and set-up uncertainty could contribute to the measured dose distributions. The box-plots for TPS predicted dose values appear to have a larger spread. This may be due to the variability in the point of measurement and the larger dose calculation grid size. Chest wall radiotherapy also showed higher surface dose compared to breast conserving radiotherapy. This was due to the application of 1.0 cm bolus which removes the skin sparing effect and shifted the target volume to the skin. There was a statistical significant difference (99% CI) in comparison of OSLD measurements (N = 90) with TPS predicted dose (N = 90; $p<0.01$) and EBT3 film measurements (N = 90; $p<0.01$).

Overall, in these clinical measurements, the dose measured agrees with results by phantom study for higher dose measured by OSLD as compared to EBT3 film and inconsistent comparison for OSLD and TPS measurements for both breast conserving and chest wall radiotherapy. Generally, the surface dose in chest wall irradiation was higher as compared to the responses of the dosimeters in breast conserving radiotherapy as the target volume and maximum dose was shifted towards the skin by the removal of

skin sparing effect in chest wall irradiation after applying 1.0 cm bolus placed on the skin. The dose differed for every patient due to different in breast separation, patient's set up and parameter of irradiation.

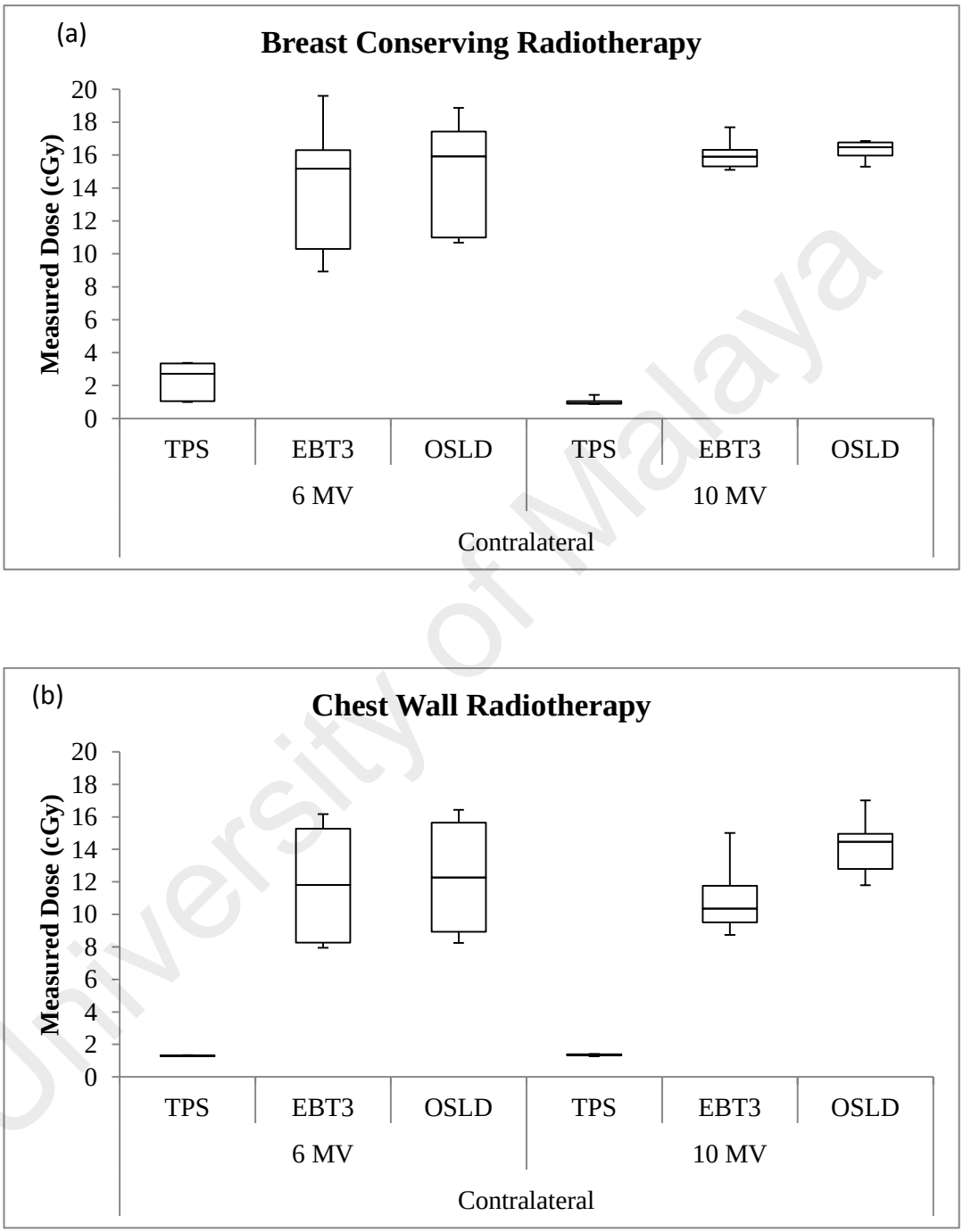

Figure 5.7: (a) Surface dose of the contralateral for breast conserving and (b) chest wall radiotherapy, respectively

Figure 5.7 shows the box-plot of the surface dose measured on the contralateral breast of the 10 patients. The box-plot shows a similar trend to the phantom study. *In-vivo* measurements using OSLD and EBT3 film measurements were found to be in good agreement with each other albeit much higher than those predicted by the TPS. Median surface dose measured was higher than 14 cGy and 10 cGy for breast conserving and chest wall radiotherapy, respectively. In comparison, the TPS predicted a median dose of less than 3 cGy. This may be because the TPS does not take into account absorbed dose due to scattered radiation. The scattered radiation from the treated breast to the contralateral breast could be as high as 18.87 cGy per fraction.

The range of contralateral dose recorded for this study agreed with previous study by other authors (Alzoubi et al., 2010; Chougule, 2007; Wahba A.G. & Safwat, 2009) which was under recommended maximum dose for the contralateral breast of not more than 3.3 Gy by Radiation Therapy Oncology Group (RTOG) breast study protocol (Alanyali et al., 2013).

5.4 Conclusion

The OSLD was found to be a suitable dosimeter for *in-vivo* dose measurements. However, we have found that the OSLD response to dose at 0.4 mm depth and thus, consequently overestimate the surface dose. The OSLD can be corrected for surface dose (Hp(0.0)) and skin dose (Hp(0.07)) by multiplying with factor of 0.42 and 0.54, respectively. In addition, the dose at the depth measure by the dosimeter may be useful in managing late skin toxicity which due to radiation effects on the skin dermis layer.

CHAPTER 6: THE APPLICATION OF Al_2O_3:C OPTICALLY STIMULATED LUMINESCENCE DOSIMETER (OSLD) FOR DOSE VERIFICATION DURING RADIOTHERAPY

6.1 Overview

In the previous chapters, the OSLD has been characterised under megavoltage photon beam (Chapter 4), as well as for surface dose measurements during radiotherapy (Chapter 5). Other than the three dimensional conformal radiation therapy (3D-CRT), arc therapies with implementation of intensity modulated radiation therapy (IMRT) and volumetric modulated arc therapy (VMAT) had provided several potential advantages over the conventional technique by improving the treatment delivery system. The techniques managed to provide highly conformal doses to the target volume and spare the surrounding tissue and organs without exceeding the tolerance limit while changing the variable of gantry speed, field size and dose rate (Korreman et al., 2009; Leybovich et al., 2003; Palma et al., 2010).

Advanced radiotherapy techniques produce radiation dose maps with high dose modulation and tight gradients which need interpolation between planning control points (Mans et al., 2010). Consequently, precise and accurate treatment verification is needed in ensuring the correct dose is being delivered to the target area during radiotherapy.

American Association of Physicists in Medicine (AAPM) Task Group No. 40 recommended that clinics should have access to TLD or other *in-vivo* system in order to prevent major treatment errors (Kutcher et al., 1994). In this chapter, the OSLD is used for dose verification in three different radiotherapy techniques namely 3D-CRT, IMRT and VMAT.

6.2 Methodology

6.2.1 Phantom and Measurement Setup

Two phantoms were used in this work. The first one is a cylindrical IMRT head and neck phantom (model 002HN, CIRS Tissue Stimulation and Phantom Technology, USA) (radius=16 cm, length=30 cm) as shown in Figure 6.1(a). The phantom consists of 5 fabricated OSLD holder rods of tissue equivalent materials with diameter of 1.27 cm and length of 15 cm. The second phantom is the pelvic section of the Atom anthropomorphic phantom (model 702-G, CIRS Tissue Stimulation and Phantom Technology, USA) as shown in Figure 6.1(b).

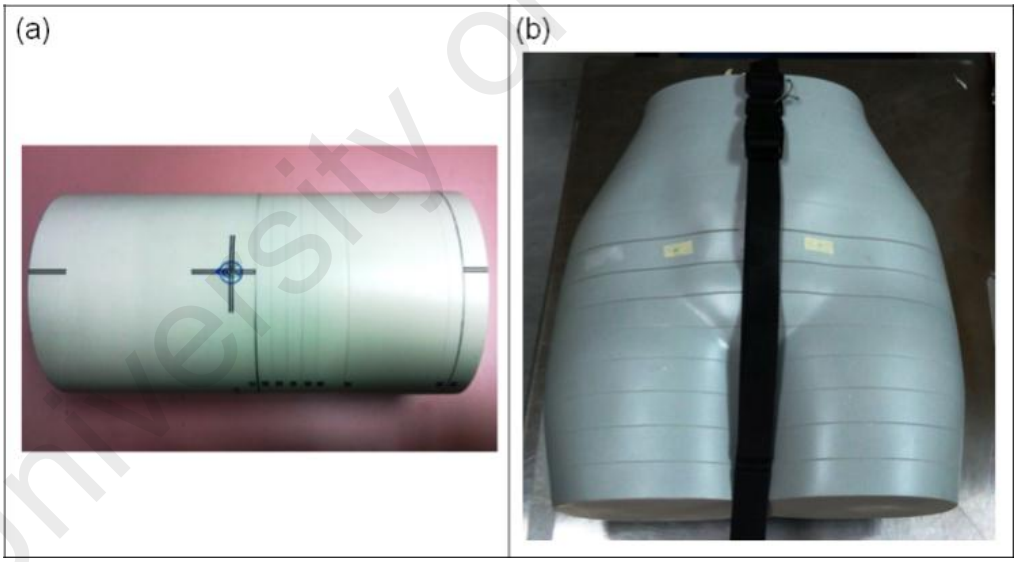

Figure 6.1: (a) The IMRT head and neck phantom and (b) pelvic section of the Atom anthropomorphic phantom, respectively

The phantoms were scanned using CT scanners (refer Section 3.1) and the CT images were then imported into the TPS. Different plans were created namely, 3D-CRT, IMRT and VMAT plans using Eclipse^{TM} TPS version 10 software (Varian Medical

System, Palo Alto, USA), XiO TPS software version 4.7 (Elekta, Maryland Heights, USA) and Monaco TPS version 3.20.01 (Elekta, Maryland Heights, USA), respectively. Details on the generation of treatment plans for 3D-CRT, IMRT and VMAT are provided in Sections 6.2.2, 6.2.3 and 6.2.4 respectively. Briefly, three types of 3D-CRT plans were designed which include plans with single direct field, parallel-opposed (two) fields and four fields. As for IMRT and VMAT, plans were designed to treat head-and-neck and prostate cancer cases.

The delivery of 3D-CRT plans and treatments were performed using a Varian Clinac 2100C/D linear accelerator (Varian Medical System, Palo Alto, USA) installed in UMMC, while the delivery of IMRT and VMAT plans were carried out at Pantai Hospital Kuala Lumpur using Elekta Synergy linear accelerator (Elekta, Maryland Heights, USA). The Planning Target Volume (PTV) and Organ at Risk (OAR) were contoured on the CT images.

In 3D-CRT plans, the OSLDs were placed at the isocentre (C-position) of the IMRT head and neck phantom (refer Figure 6.2). In the head and neck plans for both IMRT and VMAT, the OSLD was placed in the fabricated OSLD holder rods at five different positions in the phantom as shown in Figure 6.2.

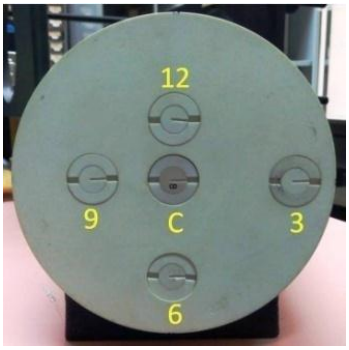

Figure 6.2: Photograph showing the IMRT head and neck phantom with the inserts for the OSLD adaptors. The positions of the adaptors were labeled with respect to the center (C) adaptor

For the prostate plans of IMRT and VMAT, the OSLD was placed in the OSLD holder at 12 different positions (refer Table 6.1) in the phantom as shown in Figure 6.3.

Table 6.1: Labels of the OSLD positions in the anthropomorphic phantom during prostate IMRT and VMAT.

Organ	Label	Positions
Intestine	a	Left anterior intestine
	b	Right anterior intestine
	c	Left posterior intestine
	d	Right posterior intestine
Spine	e	Spine
Pelvis	f	Left pelvis
	g	Right pelvis
Bladder	h	Left lateral bladder
	i	Anterior bladder
	j	Right lateral bladder
	k	Posterior bladder
Rectum	l	Rectum

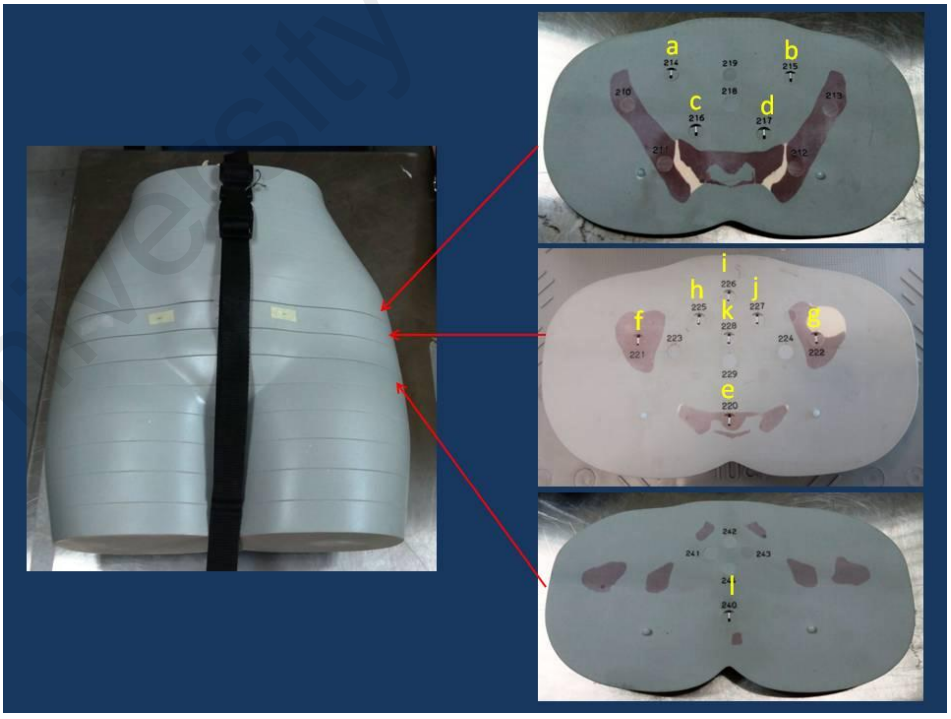

Figure 6.3: The placements of the OSLD in the pelvic section of the anthropomorphic phantom

The effect of OSLD positioning on the measured absorbed dose, with respect to their orientation (either horizontal or vertical) within the phantom was also investigated in this work. The OSLD orientation is shown in Figure 6.4.

Two sets of CT images were used. The OSLDs were first placed in the horizontal position and scanned using the CT scanner. Then, all the OSLDs were rotated 90^{o} and scanned again. The IMRT and VMAT plans were then generated on the two CT image sets. In the TPS, regions of interest (ROIs) and absorbed dose corresponding to the location of the OSLDs was contoured and recorded. It was noted that the different orientation of the OSLDs also resulted in slight offsets in the measurement location (within ±2 mm). Hence, two sets of TPS measurements were recorded. The IMRT and VMAT irradiations were carried out with the OSLD in horizontal and vertical orientations separately.

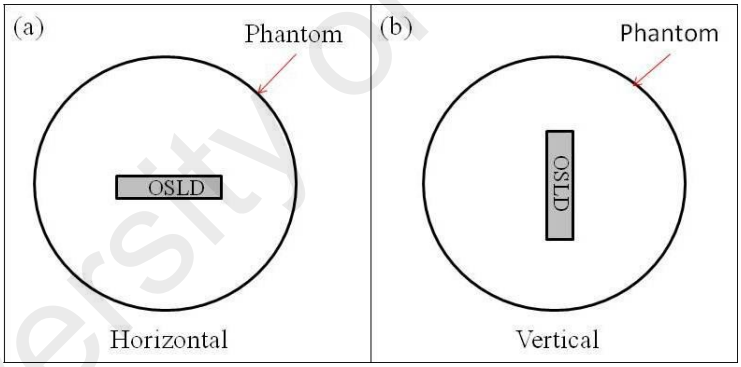

Figure 6.4: (a) The horizontal and (b) vertical orientation of OSLD, during irradiations

A MicroStar Reader (Landauer, Inc., Glenwood, IL) combined with MicroStar software, version 4.3 was used for readout of the OSLD. Data was exported in Microsoft Excel format for analysis. The OSLD measurements were compared with the TPS predicted dose.

6.2.2 3D-CRT Treatment Planning

Three 3D-CRT plans were created namely single field, parallel-opposed field and four fields irradiation using Eclipse^{TM} TPS. The TPS uses pencil beam convolution algorithm with calculation grid size of 2.5 × 2.5 mm^2. By using 6 MV photon beam with field size of 10 × 10 cm^2, a 200 cGy dose was delivered to the OSLD which was placed at the isocentre.

6.2.3 IMRT Treatment Planning

A head and neck IMRT plan was planned on the CT images of the cylindrical IMRT head and neck phantom while a prostate IMRT plan was planned on the pelvic section of the Atom anthropomorphic phantom using XiO TPS. The TPS uses superposition calculation algorithm with 2.0 × 2.0 mm^2 grid size. Step and shoot method was used during the irradiations. The parameters for plans of head and neck and prostate IMRT were summarised in Table 6.2.

Table 6.2: Summary of the parameters used in head and neck and prostate IMRT plans.

Parameters	Head and neck plan	Prostate plan
Placement of OSLD	5 positions	12 positions
Prescribed dose	212 cGy to 95% isodose lines	200 cGy to 95% isodose lines
Beam energy	6 MV	10 MV
Field sizes	7 fields	7 fields
Number of beam segments	36 to 54	32 to 48

6.2.4 VMAT Treatment Planning

Monaco TPS was used to generate head and neck and prostate VMAT plans. The TPS uses Monte Carlo calculation algorithms with calculation grid size of 2.0 × 2.0 mm^2. The parameters for head and neck and prostate VMAT plans were summarised in Table 6.3.

Table 6.3: Parameters used in head and neck and prostate VMAT plans.

Parameters	Head and neck plan	Prostate plan
Placement of OSLD	5 positions	12 positions
Prescribed dose	212 cGy to 95% isodose lines	200 cGy to 95% isodose lines
Beam energy	6 MV	10 MV
Number of beam segments	215	127
Number of arcs used	2	1
Arc angle (range)	Arc #1: 0° to 180° Arc #2: 0° to 360°	220° to 290°

6.3 Results and Discussions

6.3.1 3D-CRT plan verification

Table 6.4: Results of OSLD measurement at isocentre compared to TPS calculation with prescribed dose of 200 cGy.

Field	Mean Dose ± 1 S.D (cGy)	Difference (%)
1 single field	194.56 ± 1.63	-2.72
2-fields (parallel-opposed)	197.34 ± 3.16	-1.33
4-fields	193.67 ± 2.20	-3.16

The point dose measured by the OSLD using the head and neck phantom for the single field, 2-fields and 4-fields plans are summarised in Table 6.4. The uncertainty

represented 1 standard deviation of the mean of three OSLD measurements. The highest percentage of deviation was recorded by the 4-field irradiation, followed by the single and 2-field irradiations. The average percentage of deviation for these three types of irradiation was -2.40%.

The International Commission on Radiation Units and Measurements (ICRU) recommended that the absorbed dose to the target volume be delivered should be less than ±5% of the prescribed dose (Jones, 1994). Meanwhile, AAPM Task Group 53 and IAEA TRS 430 report stated that the acceptable criteria for external beam dose calculation in an inhomogeneous phantom should be within ±7% and 7mm (Fraass et al., 1998; IAEA, 2004).

In this study, the results of the point dose measurements for three different fields of irradiations demonstrated that the deviations between the TPS predicted dose and OSLD measurements were within -3.16% which were within the recommended values. The deviation of the measured dose by OSLD and calculated dose by TPS may be due to the slight angular dependence which is inherent anisotropy of the OSLD. The OSLD is expected to measure a lower response of 4% (Kerns et al., 2011). This is because of the partial volume effect which leads to the reduction in the dose deposited by low energy electrons. As the incident beam is perpendicular to the OSLD, the low energy electrons were able to deposit dose throughout the OSLD where the thickness is only 0.2 mm. However, when the incident beam is parallel to the OSLD (edge-on), the low energy electrons were not able to penetrate the disc, and therefore, less dose are contributed to the Al_2O_3 crystal.

6.3.2 IMRT plan verification

Table 6.5: The comparison of measured doses using OSLD with TPS predicted dose for a head and neck IMRT plan.

Positions	OSLD orientation					
	Horizontal			Vertical		
	TPS (cGy)	OSLD (cGy)	Difference (%)	TPS (cGy)	OSLD (cGy)	Difference (%)
12	112.0	114.1	1.8	108.0	105.3	-2.5
3	205.0	207.6	1.3	209.0	219.4	5.0
6	127.0	127.1	0.1	132.0	127.8	-3.2
9	165.0	161.2	-2.3	164.0	156.3	-4.7
C	133.0	135.4	1.8	133.0	137.8	3.6

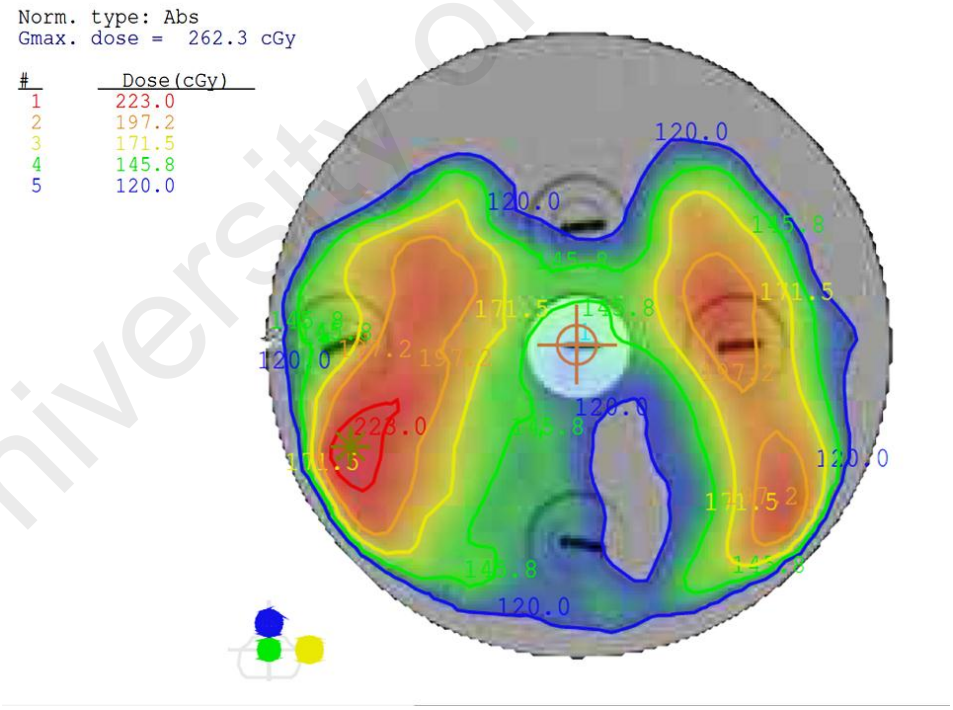

Figure 6.5: Dose colour-wash with isodose lines of the head and neck IMRT plan

Table 6.5 summarises the dose measured with the OSLD positioned in the horizontal and vertical orientation while head and neck IMRT. The dose colour-wash

for horizontal orientation of OSLD for head and neck IMRT are shown in Figure 6.5 and attached in APPENDIX F. The OSLD measurements were compared with the TPS predicted dose. The OSLD measurements were compared with the TPS predicted dose. The sign shows whether the OSLD measured a lower dose (-ve sign) or higher dose (+ve sign), with respect to the TPS predicted dose.

The measurement made using the OSLD in the horizontal orientation appears to agree better with the TPS predicted dose. The absolute mean differences were 1.5 ± 0.8% for horizontally positioned OSLD and 3.8 ± 1.0% for vertically positioned OSLD. The measurements were within the recommended values as stipulated by ICRU (±5%), AAPM and IAEA (±7%).

Comparing to 3D-CRT, the OSLD recorded bigger deviations between OSLD measurements and TPS predicted dose because of the inherent dose inhomogeneity of IMRT plans. IMRT uses inverse planning modulation and is more complex in planning and treatment systems compared to 3D-CRT. Whilst 3D-CRT plans tend to have a higher conformity index within the PTV, this may not be the case for IMRT plans. This is because IMRT plans allows for dose escalation (within PTV) to achieve better tumour control while minimizing the dose to organ at risks. As a consequence, IMRT (and VMAT) plans tend to have regions with high dose gradients. This is the reason for the increased in the deviation of the OSLD measurements and TPS predicted dose. The OSLD being a finite size detector (5 mm diameter, 0.2 mm thick) would suffer from volume averaging effect.

Table 6.6: The comparison of measured dose using OSLD with TPS predicted doses during prostate IMRT.

Labels	Positions	Horizontal			Vertical		
		TPS (cGy)	OSLD (cGy)	Difference (%)	TPS (cGy)	OSLD (cGy)	Difference (%)
a	Left anterior intestine	65.0	59.6	-8.4	65.0	60.5	-7.0
b	Right anterior intestine	58.0	58.8	1.3	62.0	64.0	3.3
c	Left posterior intestine	203.0	199.2	-1.9	201.0	199.7	-0.6
d	Right posterior intestine	202.0	189.3	-6.3	203.0	199.2	-1.9
e	Spine	125.0	129.0	3.2	127.0	128.2	1.0
f	Left pelvis	118.0	103.8	-12.0	117.0	105.9	-9.5
g	Right pelvis	89.0	94.8	6.5	86.0	84.7	-1.5
h	Left lateral bladder	148.0	127.4	-13.9	148.0	134.2	-9.3
i	Anterior bladder	75.0	70.4	-6.1	76.0	79.6	4.8
j	Right lateral bladder	133.0	131.9	-0.8	132.0	131.3	-0.5
k	Posterior bladder	219.0	197.9	-9.7	219.0	209.6	-4.3
l	Rectum	70.0	74.7	6.7	51.0	56.2	10.2

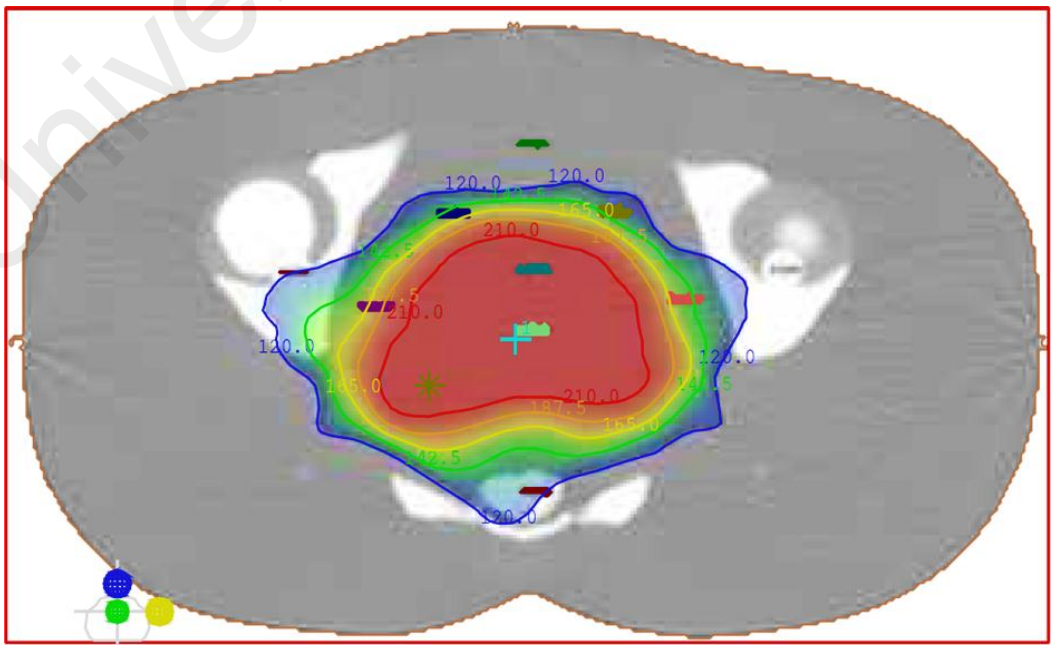

Figure 6.6: Dose colour-wash with isodose lines of the prostate IMRT plan

The dose measurements using OSLD and TPS predicted dose for horizontal and vertical orientations of OSLD during prostate IMRT were summarised in Table 6.6. Figure 6.6 shows the dose colour-wash for horizontal orientation of OSLD. The other images of the dose colour-wash during prostate IMRT were attached in APPENDIX H. Based on the table, the OSLD measurements and TPS predicted doses were different with average deviation of 6.4 ± 4.2% and 4.5 ± 3.7% for horizontal and vertical orientations, respectively.

It was noted that the deviations were bigger compared to the head and neck IMRT measurements. This was because of the difference in the phantom used. The head and neck IMRT phantom has a simpler geometry with less tissue inhomogeneities while the pelvic anthropomorphic phantom has a complex surface curvature and included various inhomogeneity such as bone and different tissue densities. Therefore, larger inhomogeneity in the dose distribution and larger dose gradients was not unexpected.

Comparing the dose for vertical and horizontal orientations, the average absolute difference of OSLD measurements was 7.1 ± 7.0%, while for TPS predicted doses was 3.6 ± 7.7%. It was noted that there were slight discrepancies between the TPS predicted dose corresponding to the position of the OSLD in the two different orientations. This indicates that even within short vicinity, IMRT plans tend to have slight dose gradients. Thus, a slight difference in the absorbed dose measured due to variation of the detector position (i.e. having the OSLDs in the horizontal or vertical orientation) is expected.

Furthermore, if the detectors happen to locate at a region where a high dose gradient is present, a larger dose difference would be possible Based on the results, there were some positions which showed large discrepancies between the OSLD measurements and the TPS predicted dose (e.g. left pelvis, left lateral bladder). On further investigation, it was found that the position of these dosimeter were at the steep

dose gradient regions, present in the vicinity of the sensitive anatomical structures in the treatment field and at the edges of the fields (Vieira et al., 2003).

6.3.3 VMAT plan verification

Table 6.7: The measurements of OSLD and TPS predicted dose during head and neck radiotherapy using VMAT.

Positions	Horizontal			Vertical		
	TPS (cGy)	OSLD (cGy)	Difference (%)	TPS (cGy)	OSLD (cGy)	Difference (%)
12	124.6	120.7	-3.2	107.4	113.9	-5.7
3	220.0	211.0	-4.1	215.5	218.4	-1.3
6	79.0	75.6	-4.3	82.0	78.8	4.1
9	178.6	171.3	-4.1	152.2	159.8	-4.8
C	133.6	128.3	-4.0	130.6	131.0	-0.3

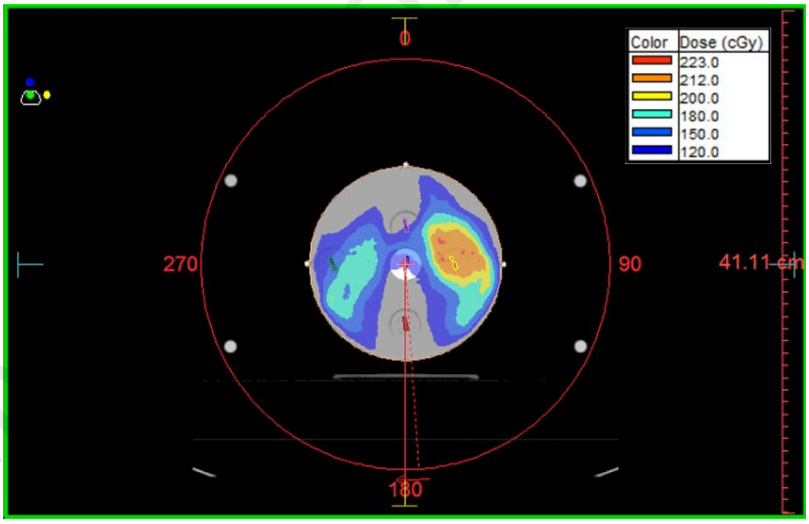

Figure 6.7: Dose colour-wash of the head and neck VMAT plan

Table 6.7 summarises the comparison OSLD measurements with the TPS predicted dose for horizontal and vertical orientation of OSLD during head and neck VMAT. Figure 6.7 shows the dose colour-wash of the OSLD during head and neck

VMAT. The dose colour-wash of head and neck VMAT for horizontal and vertical orientation of OSLD are attached in APPENDIX G.

The average deviations between OSLD measurements and TPS predicted dose were found to be within 3.94 ± 0.4% and 3.24 ± 2.3% for horizontal and vertical OSLD's orientations, respectively. The values were higher compared to the deviations measured in head and neck IMRT due to the increase in the complexity of the treatment's delivery. VMAT delivered dose while rotating the gantry simultaneously which leads to the increase in the mechanical uncertainties (Park et al., 2015).

Table 6.8: The OSLD measurements and TPS predicted dose for horizontal and vertical orientations during prostate radiotherapy using VMAT.

Labels	**Positions**	**Horizontal**			**Vertical**		
		TPS (cGy)	**OSLD (cGy)**	**Difference (%)**	**TPS (cGy)**	**OSLD (cGy)**	**Difference (%)**
a	Left anterior intestine	87.3	94.3	8.0	96.1	97.7	1.7
b	Right anterior intestine	89.8	101.9	13.4	95.5	96.4	0.9
c	Left posterior intestine	201.2	217.2	8.0	200.2	181.0	-9.6
d	Right posterior intestine	204.5	211.1	3.2	204.9	190.6	-7.0
e	Spine	67.6	57.3	-15.8	66.8	54.6	-18.3
f	Left pelvis	92.6	80.3	-13.3	88.9	73.4	-17.5
g	Right pelvis	84.1	85.0	1.0	85.8	85.8	-0.1
h	Left lateral bladder	145.5	128.5	-11.7	142.9	119.2	-16.6
i	Anterior bladder	98.8	88.4	-10.5	93.8	103.7	10.6
j	Right lateral bladder	128.2	124.4	-2.9	126.6	147.4	16.4
k	Posterior bladder	205.3	204.4	-0.4	206.2	191.1	-7.3
l	Rectum	86.7	83.9	-3.3	64.2	65.5	2.1

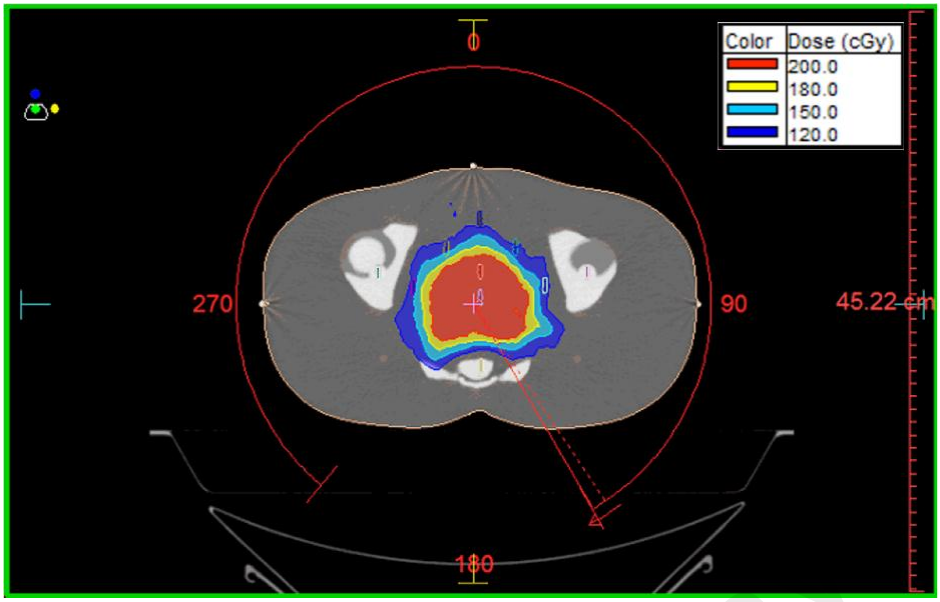

Figure 6.8: Dose colour-wash of the prostate VMAT plan

Table 6.8 shows the measured dose during prostate VMAT. The OSLD measurements were compared with TPS predicted dose for both horizontal and vertical orientation of OSLD. Figure 6.8 shows the dose colour-wash of vertical orientation of OSLD during prostate VMAT. The details of the dose colour-wash for horizontal and vertical orientations of OSLD during prostate VMAT are attached in APPENDIX I and APPENDIX J, respectively.

The OSLD measured different dose compared to TPS predicted dose with average absolute deviation of 7.6 ± 5.3% for horizontal orientation of OSLD while average absolute deviation for vertical orientation of OSLD was 9.0 ± 6.9%. The increase in complexity of planning and treatment delivery (rotational gantry movements) leads to the increase in the deviations of measured and predicted dose by OSLD and TPS, respectively.

Comparing both horizontal and vertical orientations, the OSLD measured average absolute dose difference of 3.0 ± 9.4% and TPS predicted dose differed by 3.1 ±5.7%. It is noted that the majority of the dose disagreement between the OSLD

measurements and TPS predicted dose are the positions where OSLDs were located at the steep dose gradient region.

6.4 Conclusion

In this chapter, the OSLD was used for dose verification of 3D-CRT, IMRT and VMAT plans. It was found that as the complexity of the treatment technique increased, the discrepancies between the OSLD measurements and TPS predicted doses increased. The nanoDot OSLD has an inherent angular dependency that resulted in a slight lower dose (within 4%) when used in these measurement (Kern et al., 2011). However, due to the finite size of the detector, larger discrepancies was observed for IMRT and VMAT plans as the detector may under-predict the point dose at region of high dose gradients.

Within the region where the dose is homogeneous, (eg: 3D-CRT), the uncertainty of the measurement was expected to be within 3.16 ± 2.20%. Within the regions where slight dose gradient exist (where the OSLD is near the PTV or high dose region), the uncertainty was expected to be within 6.4 ± 4.2%. At regions where large dose gradients exist (eg: borders of organ at risk or field edge of IMRT and VMAT plans), the uncertainty was expected to increase to 9.0 ± 6.0%. Care needs to be taken when scanning and during irradiations using the OSLD as a slight rotation will lead to the increase of uncertainties due to slight positional variation, thus, will result in higher difference in measured dose.

CHAPTER 7: CONCLUSION, LIMITATIONS AND FUTURE WORKS

7.1 Conclusion

In this study, a Al_2O_3:C crystal based optical OSLD (nanoDot) was characterised and used for the dosimetric verifications of selected radiotherapy techniques in megavoltage photon beams.

The first part of the study covered the characterisation of the OSLD under megavoltage radiotherapy. The OSLD exhibits a good response to function as a radiation dosimeter under megavoltage energy, showing excellent linearity and reproducibility for both 6 and 10 MV photon beams. They were also found to be minimally dependent on beam energies, dose rates, field sizes and SSDs. When used at the region of electronic equilibrium, the OSLDs were found to be minimally affected by the angulation of the detector. These characteristics showed that the OSLD is suitable to be used for clinical and *in-vivo* dose measurements.

The second part of the study covered the use of the OSLD in measuring the surface dose during radiotherapy. The OSLD was found to have a WED of 0.4 mm, compared to WED of EBT3 films (0.16 mm) and Markus ionisation chamber (0 mm). As a result, for surface dose measurement with the radiation beams perpendicularly incidence on the solid water phantom, the OSLD will measure a slightly higher dose (for OSLD, 6MV:37.77% and 10 MV: 25.38%) as compared to the Markus ionisation chamber (6MV: 15.95% and 10 MV: 12.64%) and EBT3 films (6 MV: 23.79% and 10 MV: 17.14%). In the study of the effect of incident beam angles on surface dose, it was demonstrated that surface dose increased with the increase of the incident beam angle. The OSLD and EBT3 film measurements were compared with TPS predicted dose in phantom and patient breast surface dose measurement. OSLD recorded higher dose

compared to EBT3 film for all exposures. The TPS appears to predict slightly higher dose for the treated breast while much lower dose were predicted for the contralateral breast. The measurement of the absorbed dose at a skin depth of 0.4 mm by the OSLD can be useful in preventing and managing potential acute skin reactions and late skin toxicity in radiotherapy treatments.

The last part of the study was carried out to investigate the feasibility of the OSLD in verification of the absorbed dose during selected radiotherapy techniques, namely, 3D-CRT, IMRT and VMAT irradiations. The OSLD is suitable to be used for 3D-CRT, IMRT and VMAT dose verification using suitable phantom. The OSLD is useful particularly in measuring point dose. It is useful to have knowledge on the actual absorbed dose of the positions corresponding to the tumour or organ at risk while taking into account all the variation in the body contours and tissue inhomogeneities. Within the region where the dose is homogeneous, the uncertainty of the measurement was expected to be within 3.16 ± 2.20%. Within the regions where slight dose gradient exist (where the OSLD is near the PTV or high dose region), the uncertainty was expected to be within 6.4 ± 4.2%. At regions where large dose gradients exist, the uncertainty was expected to increase to 9.0 ± 6%. Caution needs to be taken while scanning and during irradiations using the OSLD as a slight rotation will lead to the increase of uncertainties thus, will cause to higher difference measured dose.

7.2 LIMITATIONS AND FUTURE WORKS

The OSLD has several limitations when used under megavoltage beam. One of the limitations is that the OSLD has sensitive volume which was asymmetric design. Thus the OSLD need to be used in caution during irradiations which involve angles of incident beam (optimum angle to be used is 90°) as the difference in the buildup region

during the irradiations led to the difference in the dose measured. The OSLD has limitation in measuring 2D dosimetry and it only can be used for point dose measurements. Other than that, the OSLD need to be avoided from being place at the inhomogeneous and steep dose gradients regions lead to a larger deviation in dose measured. Unlike ionisation chamber which is an absolute dosimeter, the OSLD is a passive and relative dosimeter which needs periodic recalibration. The OSLD would not be suitable for real time adaptive radiotherapy measurements. However, the OSLD can still be used for inter-fraction monitoring of dose delivery.

In this work, the OSLD was used to perform *in-vivo* measurements on breast radiotherapy. Future work can extend the use of this detector in various other treatments and anatomical regions. In chapter 5, the number of patients for breast radiotherapy was confined to only five patients undergoing breast conserving radiotherapy, and five patients undergoing chest wall irradiation. This was due to the time constraint encountered during the gathering of patients with problems faced by the machines. The patients represented only a small proportion of the total number of patients undergoing breast radiotherapy at the treatment center. Therefore, research studies with a greater number of patients undergoing breast radiotherapy would be required to ensure appropriate statistics and generalisation of the findings.

Other than that, the study of the application of the OSLD in dose verification using various radiotherapy techniques was limited to the use in 3D-CRT, IMRT and VMAT only. This was because other techniques were not available at the treatment centers considered namely, University Malaya Medical Centre and Pantai Hospital Kuala Lumpur. It is recommended that the feasibility of the OSLD in dose verification during radiotherapy should be investigated for other radiotherapy techniques in future work such as image guided radiotherapy (IGRT) and stereotactic radiosurgery (SRS).

REFERENCES

Akselrod, M., Bøtter-Jensen, L., & McKeever, S. (2006). Optically stimulated luminescence and its use in medical dosimetry. *Radiation Measurements, 41*, S78-S99.

Akselrod, M., Kortov, V., & Gorelova, E. (1993). Preparation and properties of alpha-Al2O3: C. *Radiation Protection Dosimetry, 47*(1-4), 159-164.

Al-Senan, R. M., & Hatab, M. R. (2011). Characteristics of an OSLD in the diagnostic energy range. *Medical Physics, 38*(7), 4396-4405.

Alaei, P., Higgins, P. D., Weaver, R., & Nguyen, N. (2004). Comparison of dynamic and step-and-shoot intensity-modulated radiation therapy planning and delivery. *Med. Dosim., 29*(1), 1-6.

Alanyalı, S. D., Ceylan, N., & Haydaroglu, A. (2013). The Organs at Risk and Radiation Tolerance Doses *Principles and Practice of Modern Radiotherapy Techniques in Breast Cancer* (pp. 117-138): Springer.

Alzoubi, A., Kandaiya, S., Shukri, A., & Elsherbieny, E. (2010). Contralateral breast dose from chest wall and breast irradiation: local experience. *Australasian Physical & Engineering Sciences in Medicine, 33*(2), 137-144.

Andersen, C. E., Nielsen, S. K., Greilich, S., Helt-Hansen, J., Lindegaard, J. C., & Tanderup, K. (2009). Characterization of a fiber-coupled Al2O3: C luminescence dosimetry system for online in vivo dose verification during Ir-192 brachytherapy. *Medical Physics, 36*(3), 708-718.

Archambeau, J. O., Pezner, R., & Wasserman, T. (1995). Pathophysiology of irradiated skin and breast. *International Journal of Radiation Oncology Biology Physics, 31*(5), 1171-1185.

Attix, F. H. (2008). *Introduction to radiological physics and radiation dosimetry*: John Wiley & Sons.

Aznar, M., Medin, J., Hemdal, B., Klang, A. T., Bøtter-Jensen, L., & Mattsson, S. (2005). A Monte Carlo study of the energy dependence of Al2O3: C crystals for real-time in vivo dosimetry in mammography. *Radiation Protection Dosimetry, 114*(1-3), 444-449.

Barbés, B., Azcona, J. D., Burguete, J., & Martí-Climent, J. M. (2014). Application of spherical diodes for megavoltage photon beams dosimetry. *Medical Physics, 41*(1), 012102.

Bilge, H., Cakir, A., Okutan, M., & Acar, H. (2009). Surface dose measurements with GafChromic EBT film for 6 and 18MV photon beams. *Physica Medica, 25*(2), 101-104.

Borca, V. C., Pasquino, M., Russo, G., Grosso, P., Cante, D., Sciacero, P., . . . Tofani, S. (2013). Dosimetric characterization and use of GAFCHROMIC EBT3 film for IMRT dose verification. *Journal of Applied Clinical Medical Physics, 14*(2).

Bøtter-Jensen, L., Agersnap Larsen, N., Markey, B., & McKeever, S. (1997). Al_2O_3: C as a sensitive OSL dosemeter for rapid assessment of environmental photon dose rates. *Radiation Measurements, 27*(2), 295-298.

Bøtter-Jensen, L., & McKeever, S. (1996). Optically stimulated luminescence dosimetry using natural and synthetic materials. *Radiation Protection Dosimetry, 65*(1-4), 273-280.

Bøtter-Jensen, L., McKeever, S. W., & Wintle, A. G. (2003). *Optically stimulated luminescence dosimetry* (Vol. 1). Amsterdam, Netherland: Elsevier.

Bøtter-Jensen, L., & Murray, A. (2001). Optically stimulated luminescence techniques in retrospective dosimetry. *Radiation Physics and Chemistry, 61*(3), 181-190.

Bøtter-Jensen, L., Thomsen, K. J., & Jain, M. (2010). Review of optically stimulated luminescence (OSL) instrumental developments for retrospective dosimetry. *Radiation Measurements, 45*(3), 253-257.

Brenner, D. J. (2010). Contralateral second breast cancers: prediction and prevention. *Journal of National Cancer Institute 102*(7), 444-445.

Butson, M., Cheung, T., & Yu, P. (2006). Scanning orientation effects on Gafchromic EBT film dosimetry. *Australasian Physical and Engineering Sciences in Medicine, 29*(3), 281-284.

Butson, M., Perez, M., Mathur, J., & Metcalfe, P. (1996). 6MV x-ray dose in the build up region: empirical model and the incident angle effect. *Australasian Physical & Engineering Sciences in Medicine, 19*(2), 74-82.

Butson, M. J., Yu, P. K., Cheung, T., & Metcalfe, P. (2003). Radiochromic film for medical radiation dosimetry. *Materials Sciences and Engineering Reports, 41*(3), 61-120.

Chandra, B., Lakshmanan, A., Bhatt, R., & Vohra, K. (1982). Annealing and re-usability characteristics of LiF (Mg, Cu, P) TLD phosphor. *Radiation Protection Dosimetry, 3*(3), 161-167.

Chang-Claude, J., Popanda, O., Tan, X.-L., Kropp, S., Helmbold, I., von Fournier, D., . . . Schmezer, P. (2005). Association between polymorphisms in the DNA repair genes, XRCC1, APE1, and XPD and acute side effects of radiotherapy in breast cancer patients. *Clinical Cancer Research, 11*(13), 4802-4809.

Chen, F., Gupta, R., & Metcalfe, P. (2010). Intensity modulated radiation therapy (IMRT) surface dose measurements using a PTW advanced Markus chamber. *Australasian Physical and Engineering Sciences in Medicine, 33*(1), 23-34.

Cheung, T., Butson, M. J., & Peter, K. (2005). Post-irradiation colouration of Gafchromic EBT radiochromic film. *Physics in Medicine and Biology 50*(20), N281.

Chougule, A. (2007). Radiation dose to contra lateral breast during treatment of breast malignancy by radiotherapy. *Journal of Cancer Research and Therapeutics, 3*(1).

Cooper, J. S., Pajak, T. F., Forastiere, A. A., Jacobs, J., Campbell, B. H., Saxman, S. B., . . . Rotman, M. (2004). Postoperative concurrent radiotherapy and chemotherapy for high-risk squamous-cell carcinoma of the head and neck. *New England Journal of Medicine, 350*(19), 1937-1944.

Devic, S. (2011). Radiochromic film dosimetry: past, present, and future. *Physica Medica, 27*(3), 122-134.

Devic, S., Seuntjens, J., Abdel-Rahman, W., Evans, M., Olivares, M., Podgorsak, E., . . . Soares, C. G. (2006). Accurate skin dose measurements using radiochromic film in clinical applications. *Medical Physics, 33*(4), 1116-1124.

Driscoll, C., McWhan, A., O'Hagan, J., Dodson, J., Mundy, S., & Todd, C. (1986). The characteristics of new LiF preparations and sensitised LiF. *Radiation Protection Dosimetry, 17*(1-4), 367-371.

Dunn, L., Lye, J., Kenny, J., Lehmann, J., Williams, I., & Kron, T. (2013). Commissioning of optically stimulated luminescence dosimeters for use in radiotherapy. *Radiation Measurements, 51*, 31-39.

Edmund, J., Andersen, C., Marckmann, C., Aznar, M., Akselrod, M., & Bøtter-Jensen, L. (2006). CW-OSL measurement protocols using optical fibre Al_2O_3: C dosemeters. *Radiation Protection Dosimetry, 119*(1-4), 368-374.

Edmund, J. M., Andersen, C. E., & Greilich, S. (Eds.). (2007). *A track structure model of optically stimulated luminescence from Al_2O_3: C irradiated with 10–60MeV protons* (Vol. 262): Elsevier.

Eisenlohr, H., & Abedin-Zadeh, R. (1973). Checking dosimetry accuracy by post. *IAEA Bulletin*, *15*(2), 40-43.

Ezzell, G. A., & Chungbin, S. (2001). The overshoot phenomenon in step-and-shoot IMRT delivery. *J. Appl. CLin. Med. Phys.*, *2*(3), 138-148.

Fatima, N., Naqvi, M., Parveen, R., & Sajjad, Z. (2012). Radiation Dosimetry: From Thermoluminescence Dosimeter (TLD) to Optically Stimulated Luminescence Dosimeter (OSLD). *PJR, 21*(3).

Fraass, B., Doppke, K., Hunt, M., Kutcher, G., Starkschall, G., Stern, R., & Van Dyke, J. (1998). American Association of Physicists in Medicine Radiation Therapy Committee Task Group 53: quality assurance for clinical radiotherapy treatment planning. *Medical Physics*, *25*(10), 1773-1829.

Fry, R. (1992). The biological basis for dose limitation to the skin. *Japan Atomic Energy Research Institute*, 558.

Funama, Y., Taguchi, K., Utsunomiya, D., Oda, S., Murasaki, H., Yamashita, Y., & Awai, K. (2012). Dose profiles for lung and breast regions at prospective and retrospective CT coronary angiography using optically stimulated luminescence dosimeters on a 64-detector CT scanner. *Physica Medica, 28*(1), 76-82.

Gerbi, B. J., & Khan, F. M. (1990). Measurement of dose in the buildup region using fixed separation plane-parallel ionization chambers. *Medical Physics, 17*(1), 17-26.

Hamers, H., Johansson, K.-A., Venselaar, J., De Brouwer, P., Hansson, U., & Moudi, C. (1991). Entrance and exit TL-dosimetry in the conservative treatment of breast cancer: a pilot study for the EORTC-Radiotherapy Cooperative Group. *Radiotherapy and Oncology*, *22*(4), 280-284.

Hsu, S.-H., Roberson, P. L., Chen, Y., Marsh, R. B., Pierce, L. J., & Moran, J. M. (2008). Assessment of skin dose for breast chest wall radiotherapy as a function of bolus material. *Physics in Medicine and Biology*, *53*(10), 2593.

Hu, B. (2010). *Optically stimulated luminescence (OSL) and its applications in radiation therapy dosimetry*. University of Wollongong. University of wollongong Research Online.

Hunt, M. A., Kutcher, G. J., Burman, C., Fass, D., Harrison, L., Leibel, S., & Fuks, Z. (1993). The effect of setup uncertainties on the treatment of nasopharynx cancer. *International Journal of Radiation Oncology Biology Physics*, *27*(2), 437-447.

IAEA. (2004). Commissioning and quality assurance of computerized planning systems for radiation treatment of cancer. *IAEA Technical Report Series No. 430*.

IAEA. (2013). Development of Procedures for In Vivo Dosimetry in Radiotherapy. *IAEA Human Health Reports 8* Retrieved 6 March, 2015

Ismail, A., Giraud, J.-Y., Lu, G.-N., Sihanath, R., Pittet, P., Galvan, J.-M., & Balosso, J. (2009). Radiotherapy quality insurance by individualized *in-vivo* dosimetry: State of the art. *Cancer Radiotherapie*, *13*(3), 182-189.

Izewska, J., & Rajan, G. (2005). Radiation dosimeters. *Radiation Oncology Physics: A Handbook for Teachers and Students*.

Jones, D. (1994). ICRU report 50—prescribing, recording and reporting photon beam therapy. *Medical Physics*, *21*(6), 833-834.

Jong, W. L., Wong, J. H. D., Ung, N. M., Ng, K. H., Ho, G. F., Cutajar, D. L., & Rosenfeld, A. B. (2014). Characterization of MOSkin detector for in vivo skin dose measurement during megavoltage radiotherapy. *Journal of Applied Clinical Medical Physics*, *15*(5).

Jursinic, P. A. (2007a). Characterization of optically stimulated luminescent dosimeters, OSLDs, for clinical dosimetric measurements. *Medical physics*, *34*, 4594.

Jursinic, P. A. (2007b). Characterization of optically stimulated luminescent dosimeters, OSLDs, for clinical dosimetric measurements. *Medical Physics*, *34*(12), 4594-4604.

Jursinic, P. A. (2010). Changes in optically stimulated luminescent dosimeter (OSLD) dosimetric characteristics with accumulated dose. *Medical Physics*, *37*(1), 132-140.

Jursinic, P. A., & Yahnke, C. J. (2011). *In -vivo* dosimetry with optically stimulated luminescent dosimeters, OSLDs, compared to diodes; the effects of buildup cap thickness and fabrication material. *Medical Physics*, *38*(10), 5432-5440.

Kalchgruber, R., Göksu, H., Hochhäuser, E., & Wagner, G. (2002). Monitoring environmental dose rate using RiSO TL/OSL readers with built-in sources: recommendations for users. *Radiation Measurements*, *35*(6), 585-590.

Kerns, J. R., Kry, S. F., Sahoo, N., Followill, D. S., & Ibbott, G. S. (2011). Angular dependence of the nanoDot OSL dosimeter. *Medical Physics, 38*(7), 3955-3962.

Korreman, S., Medin, J., & Kjaer-Kristoffersen, F. (2009). Dosimetric verification of RapidArc treatment delivery. *Acta Oncologica, 48*(2), 185-191.

Kry, S. F., Smith, S. A., Weathers, R., & Stovall, M. (2012). Skin dose during radiotherapy: a summary and general estimation technique. *Journal of Applied Clinical Medical Physics, 13*(3).

Kutcher, G. J., Coia, L., Gillin, M., Hanson, W. F., Leibel, S., Morton, R. J., . . . Svensson, G. K. (1994). Comprehensive QA for radiation oncology: report of AAPM radiation therapy committee task group 40. *Medical Physics, 21*, 581-581.

Kwan, I. S., Rosenfeld, A. B., Qi, Z. Y., Wilkinson, D., Lerch, M. L., Cutajar, D. L., . . . Chin, Y. (2008). Skin dosimetry with new MOSFET detectors. *Radiation Measurements, 43*(2), 929-932.

Laurent, A., Mistretta, F., Bottigioli, D., Dahel, K., Goujon, C., Nicolas, J. F., . . . Laurent, P. E. (2007). Echographic measurement of skin thickness in adults by high frequency ultrasound to assess the appropriate microneedle length for intradermal delivery of vaccines. *Vaccine, 25*(34), 6423-6430.

Lee, J., Yang, J., Kim, J., Pradhan, A., Lee, J., Chung, K., & Choe, H. (2006). Dosimetric characteristics of LiF: Mg, Cu, Si thermoluminescent materials. *Applied Physics Letters, 89*(9), 094110.

Lee, S.-Y., & Jai Lee, K. (2001). Development of a personal dosimetry system based on optically stimulated luminescence of Al_2O_3: C for mixed radiation fields. *Applied Radiation and Isotopes, 54*(4), 675-685.

Lee, S.-Y., Kim, B.-H., & Lee, K. J. (2001). An application of artificial neural intelligence for personal dose assessment using a multi-area OSL dosimetry system. *Radiation Measurements, 33*(3), 293-304.

Leybovich, L. B., Sethi, A., & Dogan, N. (2003). Comparison of ionization chambers of various volumes for IMRT absolute dose verification. *Medical Physics, 30*(2), 119-123.

Madsen, A. T., & Murray, A. S. (2009). Optically stimulated luminescence dating of young sediments: a review. *Geomorphology, 109*(1), 3-16.

Malthez, A. L., Freitas, M. B., Yoshimura, E. M., & Button, V. L. (2014). Application of optically stimulated luminescence technique to evaluate simultaneously accumulated and single doses with the same dosimeter. *Radiation Physics and Chemistry*, *95*, 134-136.

Mans, A., Remeijer, P., Olaciregui-Ruiz, I., Wendling, M., Sonke, J.-J., Mijnheer, B., . . . Stroom, J. C. (2010). 3D Dosimetric verification of volumetric-modulated arc therapy by portal dosimetry. *Radiotherapy and Oncology*, *94*(2), 181-187.

Massillon-JL, G., Chiu-Tsao, S.-T., Domingo-Muñoz, I., & Chan, M. F. (2012). Energy dependence of the new Gafchromic EBT3 film: dose response curves for 50 kV, 6 and 15 MV X-ray beams. *International Journal of Radiation Oncology Biology Physics*, *1*(2), 60-65.

Mayles, P., Nahum, A., & Rosenwald, J.-C. (2010). *Handbook of radiotherapy physics: theory and practice*: CRC Press.

McKeever, S. W., Blair, M. W., Bulur, E., Gaza, R., Gaza, R., Kalchgruber, R., . . . Yukihara, E. G. (2004). Recent advances in dosimetry using the optically stimulated luminescence of Al2O3: C. *Radiation Protection Dosimetry*, *109*(4), 269-276.

McKeever, S. W., Moscovitch, M., & Townsend, P. D. (1995). *Thermoluminescence dosimetry materials: properties and uses*. Ashford: Nuclear Technology Publications.

McQuestion, M. (2006). *Evidence-based skin care management in radiation therapy.* Paper presented at the Seminars in Oncology Nursing.

Mijnheer, B., Beddar, S., Izewska, J., & Reft, C. (2013). *In-vivo* dosimetry in external beam radiotherapy. *Medical Physics*, *40*(7), 070903.

Murray, A., & Funder, S. (2003). Optically stimulated luminescence dating of a Danish Eemian coastal marine deposit: a test of accuracy. *Quaternary Science Reviews*, *22*(10), 1177-1183.

Murray, A. S., & Roberts, R. G. (1997). Determining the burial time of single grains of quartz using optically stimulated luminescence. *Earth and Planetary Science Letters*, *152*(1), 163-180.

Neves, L. P., Perini, A. P., dos Santos, G. P., Xavier, M., Khoury, H. J., & Caldas, L. V. (2012). Characterization of a homemade ionization chamber for radiotherapy beams. *Applied Radiation and Isotopes*, *70*(7), 1291-1295.

Northcliffe, L. C., & Schilling, R. (1970). *Range and stopping-power tables for heavy ions* (Vol. 7): Atomic Data and Nuclear Data Tables.

Olley, J., Caitcheon, G. G., & Roberts, R. (1999). The origin of dose distributions in fluvial sediments, and the prospect of dating single grains from fluvial deposits using optically stimulated luminescence. *Radiation Measurements, 30*(2), 207-217.

Palma, D. A., Verbakel, W. F., Otto, K., & Senan, S. (2010). New developments in arc radiation therapy: a review. *Cancer Treatment Reviews, 36*(5), 393-399.

Park, J. M., Wu, H.-G., Kim, J. H., Carlson, J. N., & Kim, K. (2015). The effect of MLC speed and acceleration on the plan delivery accuracy of VMAT. *The British Journal of Radiology, 88*(1049), 20140698.

Perks, C. A., Yahnke, C., & Million, M. (2008). Medical dosimetry using Optically Stimulated Luminescence dots and microStar readers. Retrieved from

Pisani, L., Lockman, D., Jaffray, D., Yan, D., Martinez, A., & Wong, J. (2000). Setup error in radiotherapy: on-line correction using electronic kilovoltage and megavoltage radiographs. *International Journal of Radiation Oncology Biology Physics, 47*(3), 825-839.

Podgorsak, E. (2005). *Radiation oncology physics: A handbook for teachers and students* (Vol. 1). Vienna: IAEA Publications.

Podgorsak Ervin, B. (2003). *Review of Radiation Oncology Physics: A Handbook for Teachers and Students* Vienna: IAEA Publications.

Rawlinson, J. A., Arlen, D., & Newcombe, D. (1992). Design of parallel plate ion chambers for buildup measurements in megavoltage photon beams. *Medical Physics, 19*(3), 641-648.

Reft, C. S. (2009a). The energy dependence and dose response of a commercial optically stimulated luminescent detector for kilovoltage photon, megavoltage photon, and electron, proton, and carbon beams. *Medical Physics, 36*(5), 1690-1699.

Reft, C. S. (2009b). The energy dependence and dose response of a commercial optically stimulated luminescent detector for kilovoltage photon, megavoltage photon, and electron, proton, and carbon beams. *Medical physics, 36*, 1690.

Rosenfeld, A. B. (Ed.). (2011). *Advanced Semiconductor dosimetry in radiation therapy* (Vol. 1). Melville, N.Y.: American Institute of Physics.

Scalchi, P., & Francescon, P. (1998). Calibration of a MOSFET Detection System for 6-MV *in-vivo* Dosimetry. *International Journal of Radiation Oncology Biology Physics, 40*(4), 987-993.

Schembri, V., & Heijmen, B. (2007). Optically stimulated luminescence (OSL) of carbon-doped aluminum oxide (Al2O3: C) for film dosimetry in radiotherapy. *Medical Physics, 34*(6), 2113-2118.

Sim, G., Wong, J., & Ng, K. (2013). The use of radiochromic EBT2 film for the quality assurance and dosimetric verification of 3D conformal radiotherapy using Microtek ScanMaker 9800XL flatbed scanner. *Journal of Applied Clinical Medical Physics, 14*(4).

Sivakumar, S., Krishnamurthy, K., Davis, C., Ravichandran, R., Kannadhasan, S., Biunkumar, J., & El Ghamrawy, K. (2008). Clinical implementation of dynamic intensity-modulated radiotherapy: Dosimetric aspects and initial experience. *Journal of Medical Physics/Association of Medical Physicists of India, 33*(2), 64.

Sommer, M., Jahn, A., & Henniger, J. (2011). A new personal dosimetry system for Hp(10) and Hp(0.07) photon dose based on OSL-dosimetry of beryllium oxide. *Radiation Measurements, 46*(12), 1818-1821.

Sorriaux, J., Kacperek, A., Rossomme, S., Lee, J. A., Bertrand, D., Vynckier, S., & Sterpin, E. (2013). Evaluation of Gafchromic® EBT3 films characteristics in therapy photon, electron and proton beams. *Physica Medica, 29*(6), 599-606.

Stovall, M., Smith, S. A., Langholz, B. M., Boice Jr, J. D., Shore, R. E., Andersson, M., . . . Lynch, C. F. (2008). Dose to the contralateral breast from radiotherapy and risk of second primary breast cancer in the WECARE study. *International Journal of Radiation Oncology Biology Physics, 72*(4), 1021-1030.

Van Herk, M. (2004). *Errors and margins in radiotherapy*. Paper presented at the Seminars in radiation oncology.

Van Vloten, W. A., Hermans, J., & Van Daal, W. A. (1987). *Radiation induced skin cancer and radiodermatitis of the head and neck*. Cancer, (59, 3).

van Vulpen, M., Field, C., Raaijmakers, C. P., Parliament, M. B., Terhaard, C. H., MacKenzie, M. A., . . . Fallone, B. G. (2005). Comparing step-and-shoot IMRT with dynamic helical tomotherapy IMRT plans for head-and-neck cancer. *Int. J. Radiat. Oncol. Bio. Phys. , 62*(5), 1535-1539.

Viamonte, A., Da Rosa, L., Buckley, L., Cherpak, A., & Cygler, J. (2008). Radiotherapy dosimetry using a commercial OSL system. *Medical Physics, 35*(4), 1261-1266.

Vieira, S., Dirkx, M., Pasma, K., & Heijmen, B. (2003). Dosimetric verification of x-ray fields with steep dose gradients using an electronic portal imaging device. *Physics in Medicine and Biology, 48*(2), 157.

Wahba A. G., & Safwat, R. (2009). Radiation Doses to Contralateral Breast During Irradiation of Breast Cancer. *Medical Journal of Cairo University 77*(2).

Wintle, A. G., & Murray, A. S. (2006). A review of quartz optically stimulated luminescence characteristics and their relevance in single-aliquot regeneration dating protocols. *Radiation Measurements, 41*(4), 369-391.

Wolff, D., Stieler, F., Welzel, G., Lorenz, F., Abo-Madyan, Y., Mai, S., . . . Wenz, F. (2009). Volumetric modulated arc therapy (VMAT) vs. serial tomotherapy, step-and-shoot IMRT and 3D-conformal RT for treatment of prostate cancer. *Radiotherapy and Oncology, 93*(2), 226-233.

Yadav, B. S., Sharma, S. C., Patel, F. D., Ghoshal, S., & Kapoor, R. K. (2008). Second primary in the contralateral breast after treatment of breast cancer. *Radiotherapy and Oncology, 86*(2), 171-176.

Yahnke, C. J. (2009). Calibrating the microStar. In D. o. Technology (Ed.), *InLight Systems*: Landauer.

Yasuda, H., & Kobayashi, I. (2001). Optically stimulated luminescence from Al2O3: C irradiated with relativistic heavy ions. *Radiation Protection Dosimetry, 95*(4), 339-343.

Yoshimura, E., & Yukihara, E. (2006). *Optically stimulated luminescence: searching for new dosimetric materials.* Paper presented at the 13th International Conference on Radiation Effects in Insulators, Jaipur.

Yukihara, E., Mardirossian, G., Mirzasadeghi, M., Guduru, S., & Ahmad, S. (2008). Evaluation of Al2O3: C optically stimulated luminescence (OSL) dosimeters for passive dosimetry of high-energy photon and electron beams in radiotherapy. *Medical Physics, 35*(1), 260-269.

Yukihara, E., Ruan, C., Gasparian, P., Clouse, W., Kalavagunta, C., & Ahmad, S. (2009). An optically stimulated luminescence system to measure dose profiles in x-ray computed tomography. *Physics in Medicine and Biology, 54*(20), 6337.

Yukihara, E., Sawakuchi, G., Guduru, S., McKeever, S., Gaza, R., Benton, E., . . . Kitamura, H. (2006). Application of the optically stimulated luminescence (OSL) technique in space dosimetry. *Radiation Measurements, 41*(9), 1126-1135.

Yukihara, E., Whitley, V., McKeever, S., Akselrod, A., & Akselrod, M. (2004). Effect of high-dose irradiation on the optically stimulated luminescence of Al_2O_3: C. *Radiation Measurements, 38*(3), 317-330.

Z. Maseeh, F. N., N. Mansoor, P. Riffat, S. Zafar. (2011). Radiation Dosimetry: From Thermoluminescence Dosimeter (TLD) to Optically Stimulated Luminescence Dosimeter (OSLD). *Pakistan Journal of Radiology, 21*(3), 107.

Zacharias, N., Stuhec, M., Knezevic, Z., Fountoukidis, E., Michael, C., & Bassiakos, Y. (2007). *Low-dose environmental dosimetry using Thermo-and Optically Stimulated Luminescence.* Paper presented at the 10 th International Symposium on Radiation Physics ISRP 10, Coimbra, Portugal.

Ziegler, J. F. (2013). *The stopping and ranges of ions in matter* (Vol. 6). New York: Springer.

LIST OF PUBLICATIONS AND PAPERS PRESENTED

1. "On the Use of Optically Stimulated Luminescent Dosimeter for Surface Dose Measurement during Radiotherapy" published in PLOS ONE (PLoS ONE 10(6): e0128544, DOI:10.1371/journal.pone.0128544), 2015.

2. "Surface Dose Measurements Using Optically Stimulated Luminescence Dosimeter (OSLD) During Radiotherapy" presented in 14th Asia-Oceania Congress of Medical Physics & 12th South East Asia Congress of Medical Physics (AOCMP/SEACOMP 2014) in Ho Chi Minh City, Vietnam, October, 23-25, 2014.

3. "Surface dose measurement using optically stimulated luminescence dosimeter (OSLD) during radiotherapy" presented in Postgraduate Research Seminar at University of Malaya, September 5th, 2014.